



Contact stiffness of jointed interfaces: A comparison of dynamic substructuring techniques with frictional hysteresis measurements

Verena Gimpl^{a,b,*}, Alfredo Fantetti^{a,**}, Steven W.B. Klaassen^b,
Christoph W. Schwingshackl^a, Daniel J. Rixen^b

^a Department of Mechanical Engineering, Imperial College London, Exhibition Rd, SW7 2BU, London, UK

^b Technische Universität München, Institute for Applied Mechanics, Boltzmannstr. 15, 85748 Garching, Germany

ARTICLE INFO

Communicated by H. Ouyang

Keywords:

Frequency based substructuring
Friction contact parameters
Hysteresis loop
Tangential contact stiffness
Non-linear dynamic analysis
Jointed structures

ABSTRACT

The tangential contact stiffness is an important parameter used in non-linear dynamic analyses of jointed structures since it can strongly affect the prediction of resonance frequencies. Many experimental techniques are available for contact stiffness estimations, but the reliability of such estimations remains unknown due to a lack of comparative studies. This paper proposes a comparative study of contact stiffness measurements obtained with two experimental techniques: hysteresis loop measurements and Frequency Based Substructuring (FBS). Hysteresis loops are traditionally measured with dedicated friction test rigs to provide, amongst others, contact stiffness estimations through local interface measurements. The assumption with hysteresis measurements is that the measured parameters are independent of the dynamics of the test rig and can therefore be used as input for analyses of other structures, as long as loading conditions and contact interfaces are comparable. An alternative approach to identify the contact stiffness is FBS, which uses information from the overall system dynamics. FBS has the advantage that it can be applied to any structure, without the need of building ad-hoc test rigs, consequently giving a structure-specific information. Despite this advantage over hysteresis measurements, it is as of yet not well understood how accurately FBS can extract contact stiffness values. This paper presents FBS measurements and hysteresis loop measurements performed simultaneously on the same contact interface of a traditional high-frequency friction rig during vibration, thus enabling a cross-validation of the results of both techniques. This novel comparison validates FBS approaches against local hysteresis measurements and shows the strengths and limitations of both experimental methods, making it possible to improve the current understanding of the contact stiffness of jointed structures.

1. Introduction

Complex engineering assemblies such as turbo-machinery and automobiles employ thousands of joints that connect components together. Although these joints show in most cases linear behavior, they can introduce non-linearities due to frictional contacts when vibrations exceed certain limits [1]. These frictional contacts introduce flexibility and damping due to energy dissipation and consequently have a strong influence on the structural dynamic response, which, if not accurately predicted, may lead to unwanted vibrations with risks of high cycle fatigue failures. Thus, the accurate modeling of frictional contacts is of utmost importance to

* Corresponding author at: Technische Universität München, Institute for Applied Mechanics, Boltzmannstr. 15, 85748 Garching, Germany.

** Corresponding author.

E-mail addresses: verena.gimpl@outlook.de (V. Gimpl), a.fantetti@imperial.ac.uk (A. Fantetti).

obtain reliable simulations, needed to optimize designs and predict the life of components. However, modeling the friction behavior of such contacts is a challenging task since the underlying physics is not yet fully understood. As a current work around, several experimental techniques are available to obtain friction information on the contact interfaces during vibration. However, they all have their inherent limitations that prevent the full understanding of the underlying physics.

A common practice to describe frictional contacts is by means of hysteresis loop measurements [2]. Hysteresis loops are load–deflection curves between two sliding components and can provide information on friction coefficient, tangential contact stiffness and dissipated energy, which are used to replicate the frictional behavior. To obtain hysteresis loops for non-linear dynamic analysis, high-frequency friction rigs [2–8] are needed to measure the relative displacement and the transmitted friction force between two contacting interfaces. The relative displacement can be determined by using contactless sensors, e.g. Laser-Doppler Vibrometers (LDVs) [3,4,9] or high-speed cameras with Digital Image Correlation (DIC) [7,10–14]. These methods cannot determine the relative displacement directly at the contact interface, due to its inaccessibility, but only provide information from the edges of the contacting components. Care should be taken to perform measurements as close as possible to the interface to obtain information mainly from the interface, thus minimizing the bulk material influence. The measurement of hysteresis loops also requires the determination of the friction force, which can be measured with purposely designed friction rigs. The requirement of friction rigs limits the types of joints that can be investigated, although a potential advantage is that these rigs provide input data that can generally be applied to all types of explicitly modeled non-linear systems. However, this is only valid under the assumption that the measured contact parameters are independent of the dynamics of both friction rig and studied system, while depend only on the type of joint, material pairing, and loading conditions, such as normal load and excitation force.

Other techniques that obtain information from the contact interface include ultrasound measurements [15–19] and optical measurements [20–22]. Both techniques allow direct access to the interface and, hence, more direct measurements. Unfortunately, the interpretation of the data is still very challenging due to a lack of understanding of how the small amplitude interface data can be related to real large-scale joints. Furthermore, the optical methods require transparent materials, which are not commonly used in engineering applications.

The above experimental techniques obtain information on the contact stiffness with local contact measurements. However, information on the contact stiffness can also be obtained with global dynamic forced response measurements. In the most basic way, contact parameters of a numerical model can be tuned to match predicted and measured Frequency Response Functions (FRFs). For example, Ahmadian et al. [23] modeled the joint as a combination of non-linear and linear springs and a viscous damper and tuned these parameters to match the experimental FRF. In other studies [24], the bolt stiffness and contact stiffness were modeled as thin layer elements and their values tuned to match the experimental FRF. This approach normally focuses on the most relevant resonant frequencies and implies that a fully assembled test structure is available.

An alternative technique that uses information from the overall system dynamics to identify the flexibility at the joint is Dynamic Substructuring (DS). DS includes several versatile and promising approaches to extract system information from measured data. A short overview of the history of DS is given e.g. in [25]. The principle of DS is that it decomposes the assembly into several parts, so-called substructures, which are easier to analyze and are then combined, in a so-called coupling procedure, to give information on the dynamic behavior of the assembly [25,26]. DS can be applied in different domains [26], but for vibration analysis the frequency domain is the most convenient, since frequency response functions (FRFs) can be easily measured and the methods for post-processing are relatively simple to implement. Furthermore, numerically and experimentally obtained data can be combined (hybrid approaches) making it possible to obtain information on degrees of freedom (DoFs) where measurements are difficult to perform. The use of FRFs to characterize component's properties by decomposing and coupling systems has been developed over years. One of the first attempts was made by Crowley et al. in the 1980s, who proposed a method called SMURF (structural modification using experimental frequency response functions) [27]. A few of years later the Frequency Based Substructuring (FBS) method gained popularity with the study of Jetmundsen et al. [28].

In the context of contact parameter estimation, it is assumed that the difference between the parts merged at their interfaces and the jointed assembly arises only due to the presence of the joints that combine the parts into the assembly. Thus, if the dynamic behaviors of the assembly and its parts are known, the joint properties can be identified without the need of directly accessing the interface via a so-called decoupling. Nowadays, FBS decoupling for the purpose of joint identification has attracted quite some attention due to its potential ease of use in real structures, although it is sensitive to measurement noise. FBS can identify only linear joints, due to its nature. However, a study from [29] needs to be mentioned that has made a first attempt to identify non-linear joints by using time dependent FRFs. In this study here, the focus lies on linear joints. A short summary of previous studies is given in the following. Häußler et al. [30] determined dynamic stiffness values of rubber isolators that connected two stiff crosses, via two different FBS approaches: Primal Decoupling and Inverse Substructuring [31]. They compared the results to measurements on a hydraulic testing machine and found good agreements with the axial and radial stiffness values from Primal Decoupling. They also showed that the standard Inverse Substructuring approach and its underlying assumptions did not work for their structure, and proposed two extensions to compensate for these assumptions and adapt Inverse Substructuring to more general joint cases. El Mahmoudi et al. [32] summarized approaches on how connection elements (interface compliance) can be included in FBS, with applications to rubber bushings of a vehicle. Other studies used FBS approaches to determine contact parameters of jointed connections. Tol et al. [33] investigated bolted beam structures to determine joint properties by means of a decoupling. Their proposed approach leads to four equations using different sets of measured data. The most practical of these equations is that they do not need information on the interface in the assembly configuration. Because the results are affected by numeric instabilities, they proposed in [34] an optimization algorithm that uses a selected and averaged set of the results of the decoupling approach as initial values. The optimization algorithm follows the idea of model updating by minimizing the difference between a measured and

regenerated FRF. A combination of measured assembly data (for joint observation), updated numerical models, and optimization algorithm is used in a method proposed by Klaassen et al. [35], called System Equivalent Model Mixing (SEMM), to determine joint properties without the need of measuring DoFs at the interface. The performance and difficulties of SEMM were shown in [36].

The obtained stiffness values in the mentioned studies were mostly validated indirectly, by comparing predicted and measured FRFs. Instead, in this paper, the investigated FBS methods are validated against local contact stiffness measurements. This has been achieved by applying FBS techniques to a traditional friction test rig that measures hysteresis loops. FBS measurements were performed simultaneously with hysteresis measurements, on the same contact interface during vibration, thus making a cross-validation of both techniques possible. This novel comparison has not been attempted before to the best of the authors' knowledge. Another goal of this study is to understand how the vibration behavior of jointed structures is related to their contact properties. The obtained parameters from hysteresis loops might be clouded by the friction rig's own dynamics, while FBS decoupling approaches can theoretically eliminate the structure's properties such that only properties of the joint remain. To account for the known difficulties in terms of measurement noise, four different FBS approaches were conducted, namely three decoupling approaches and the Inverse Substructuring approach, and their results compared. The method that gave the cleanest results is presented in the following sections, while the other approaches are described in the [Appendix A](#).

2. Frequency based dynamic substructuring to study the contact interface

In this study, Frequency Based Substructuring (FBS) is used to determine the contact stiffness of the contacting specimens in a friction rig under fully stuck condition. A fully stuck condition is investigated since FBS assumes linear(ized) and time-invariant structures that are in steady-state and, therefore, can only determine linear(ized) joints.

This section provides a relatively short overview of the FBS theory to provide the reader with enough background information to facilitate the interpretation of the experimental findings. For more detailed information, the reader is referred to the vast amount of available literature, e.g. [37]. In FBS, it is convenient to make a distinction between joint and interface. The joint is a source of dynamics and can have mass, stiffness and damping while the interface is a set of DoFs between which the joint acts.

FBS describes a system by means of its parts. In the context of contact parameter estimation, it is assumed that the difference between the parts merged at their interfaces and the jointed assembly is caused by the joints that combine the parts into the assembly. This is true in an ideal world. In reality, measurement noise and other errors, such as errors in the location of sensors and actors, make it difficult to apply this approach with high accuracy. This has led to the development of a series of different approaches, whose reliability also depend on the joint-type and structure. Often, it is not known beforehand which technique works the best for the investigated joint and, thus, comparative studies are conducted. In this study, four different approaches were investigated but only the approach that provided the best contact stiffness estimations is described, while the others are summarized in the [Appendix A](#).

To explain the theory of the used method, an example assembly AJB is used that consists of the substructures A and B, and the joint J. Furthermore, the ideas are visualized in [Fig. 1](#). The dynamic behavior of any structure S can be described by its admittance matrix $Y^{(S)}$, also called dynamic flexibility matrix. $Y^{(S)}$ contains the frequency response functions (FRFs) of its structure, which can be obtained experimentally, e.g. through impact tests. In its basic form, FBS assumes that if the $Y^{(S)}$ matrices of the parts A and B are known, the dynamic properties $Y^{(AJB)}$ of the assembly AJB can be determined via a so-called coupling procedure, where a spring-damper system between the substructures accounts for contact compliance and models the joint J, see [Fig. 1a](#). This leads to the so-called compliance coupling Eq. (1).

$$\tilde{Y}^{(AJB)}(\omega) = Y(\omega) - Y(\omega)B^T \left(BY(\omega)B^T + Y^{(J)}(\omega) \right)^{-1} BY(\omega) \quad (1)$$

The tilde symbol in $\tilde{Y}^{(AJB)}$ means that the assembly was derived via an equation, instead $Y^{(AJB)}$ contains measured data from the assembly. The matrix Y contains the admittance matrices of the substructures, $Y^{(A)}$ and $Y^{(B)}$, in block diagonal form. The derivation of Eq. (1) is based on (i) a weakened compatibility condition due to the spring-damper system, and (ii) a force equilibrium. The former is expressed by $Bu = \Delta u = u_c^{(A)} - u_c^{(B)}$, where B is a signed Boolean matrix that couples the DoFs and $u_c^{(S)}$ are the displacements of the interface DoFs. The weakened compatibility condition introduces a gap between the interface DoFs, which itself introduces forces in the joint. This can be expressed by $\Delta u = Y^{(J)}(\omega)\lambda$, where λ are the forces between the coupled DoFs on each side of the interface. These forces satisfy action-reaction. This means the forces on each side of the interface are equal in magnitude and opposite in sign. Consequently, the joint must be mass-less since a mass in the joint could introduce a difference of forces between DoFs of a link. This is an important property since it limits the type of joints that can be investigated. It is important to note that Eq. (1) stores the interface DoFs and thus the joint information multiple times. A detailed derivation of Eq. (1) can be found e.g. in [32]. For clarity, the frequency dependency is omitted in what follows.

The matrix of interest in this study is the inverse of $Y^{(J)}$, which represents the interface compliance as a mass-less joint with contact stiffness $K^{(J)}$ and damping $C^{(J)}$:

$$\left(Y^{(J)} \right)^{-1} = Z^{(J)} = i\omega C^{(J)} + K^{(J)} \quad (2)$$

Here, only the stiffness values are of interest and thus, only the real part of $Z^{(J)}$ is investigated: $real(Z^{(J)}) = K^{(J)}$. Some properties of $K^{(J)}$ are: (i) it is a square matrix with the size of number of couplings between interface DoFs, (ii) it can be frequency dependent, (iii) it is a diagonal matrix in case the compliance is only coupling pairs of nodes across the interface and cross-coupling between the different DoFs is neglected.

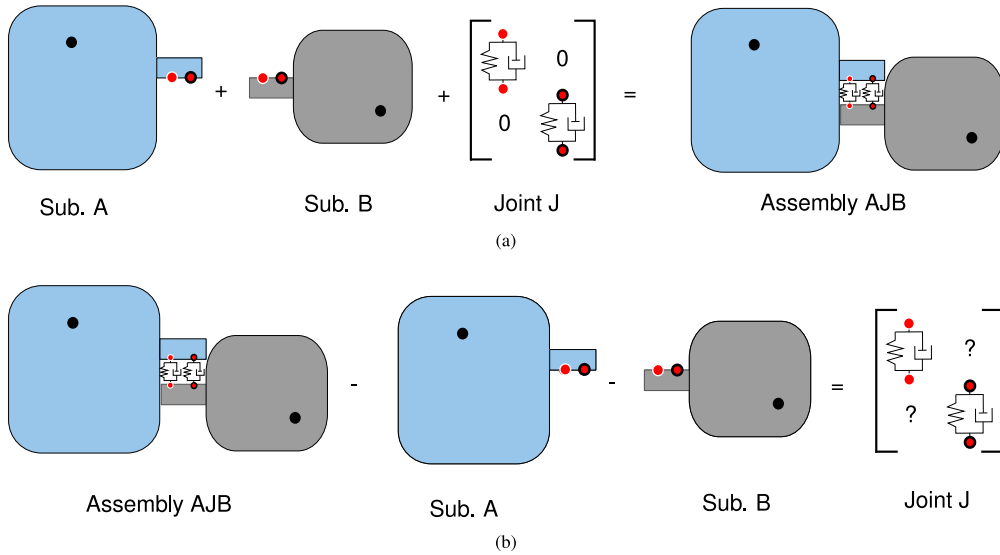


Fig. 1. Visualization of compliance coupling and decoupling: The assembly AJB consists of two substructures A and B and the joint J. The black dots represent internal DoFs i , and the red dots the interface DoFs c between which the joint acts. (a) Compliance coupling: The two substructures are coupled with a flexible joint, indicating a “weak interface”, e.g. the joint consists of springs and dampers and is assumed to be massless. In this figure only DoFs across the interface are coupled and cross-coupling is neglected leading to diagonal $Z^{(J)}$ and $Y^{(J)}$, which means that the spring-damper systems act in parallel. (b) Decoupling approaches can be used to identify the properties of the joint by eliminating the dynamics of the substructures from the assembly’s dynamics. The resulting matrix is generally a full matrix.

The compliance coupling can be seen as basis for the decoupling approaches. Decoupling approaches directly give frequency dependent information of the joint. The idea is that when the $Y^{(S)}$ of the assembly and the substructures are known, any differences are due to the joint, see Fig. 1b. In other words, when the contributions of the individual substructures on the assembly response are removed, only the property of the joint remains. The idea is simple but the pitfall with decoupling is that it is extremely sensitive to measurement errors and noise [38]. Researchers have developed different algorithms to address this problem. In this study, three decoupling approaches were investigated but only the approach that provided the best contact stiffness estimation is presented here. Results of the other two investigated decoupling approaches and an approach called *Inverse Substructuring* are presented in the Appendix A.

The approach used here was proposed by Tol et al. [34] and is based on a rearranging of Eq. (1) to determine $Y^{(J)}$, resulting in a set of four equations. The most suitable equation of this set, regarding the conducted measurements, was used in this study as Eq. (3). Because Eq. (3) is derived from Eq. (1), which assumes a mass-less joint, this assumption also applies here. Furthermore, it is to be noted that this approach does not compress the joint information because each equation of these four investigates only a sub-matrix of $Y^{(AJB)}$ that contains the joint information only once.

$$Y^{(J)} = Y_{c,i}^{(A)} \left(Y_{i(B),i(A)}^{(AJB)} \right)^{-1} Y_{i,c}^{(B)} - Y_{c,c}^{(A)} - Y_{c,c}^{(B)} \tag{3}$$

This approach uses additional internal DoFs, denoted with the subscript i , from assembly and substructures, which can be much more easily measured than interface DoFs and give in general FRFs of better quality. In Eq. (3) the number of internal DoFs within both substructures is the same. Furthermore, there is no limitation on the number of internal DoFs and it can be used with only one internal DoF per substructure. In order to obtain the frequency dependent contact stiffness matrix $K^{(J)}$ from $Y^{(J)}$, the latter matrix needs to be inverted and its real part determined.

In what follows, Eq. (3) is referred to as *decoupling interface and internal DoFs* to highlight that the joint properties are obtained from interface and internal admittances. The advantage of Eq. (3) is that it does not require information about the interface in the assembly, which can be difficult, if not impossible to determine experimentally. However, data on the interface in the disassembled state is needed. Since the investigated interface is too small for conducting measurement, a Virtual Point Transformation (VPT) [26] is used as a solution, which is described in more detail in Section 3.2.

3. Experimental methods

For this study, FBS measurements were performed on a friction rig that is normally used to measure hysteresis loops for non-linear dynamic analysis. Both FBS and hysteresis measurements were used simultaneously to extract tangential contact stiffness values. This section describes the friction rig and the FBS experimental set-up together with the experimental plan.

3.1. Description of the friction rig and hysteresis loop

The friction rig of this study is sketched in Fig. 2a and described more in detail in [9]. The rig generates an oscillating motion between two specimens with a nominally flat contact interface. At the same time, the relative displacement of the specimens and the transmitted friction force are measured simultaneously to provide hysteresis loops.

For the FBS study, the friction rig has been split into the two substructures, A and B, each consisting of several parts. Substructure A (blue colored in Fig. 2a) contains the moving parts of the rig, and substructure B (gray colored in Fig. 2a) the static parts. Substructure A consists of the moving arm that holds one specimen, and a moving inertia mass that is grounded via two leaf-springs, which enable a horizontal movement during excitation. Arm and mass are connected via a knife-edge that ensures that a normal load can be applied to the contact interface without any moment generated by bending of the arm and enables the transmission of the excitation force F_{ex} from the inertia mass to the arm. The knife edge is connected to the moving arm via 12 springs that pre-load the knife edge with 400 N normal force, which is considered large enough to minimize the edge stiffness non-linearity potentially induced during vibration loading and unloading cycles, such that it can be assumed as a linear joint. Substructure A is excited by an electrodynamic shaker (DataPhysics V20) that is attached to the moving mass via a stinger. The stinger assures that the moving mass is excited only horizontally. Substructure B consists of a static arm that holds the second specimen. Substructure B is assumed to be rigid and is grounded via three load cells that measure the friction force T , which is transmitted through the contact interface of the specimens. Each specimen is fixed in a clamp via tightening screws. The specimens are cylindrical and have a flat contact interface arranged crosswise as shown in Fig. 2b. They are named specimen A and specimen B in line with the substructure they are attached to. A pneumatic actuator assures a continuous contact between the specimens by applying a predefined constant normal load N . The load is transmitted through a push rod from the actuator to the specimens. A second push rod below the static arm avoids large bending motions of the arms and transmits the normal load to the ground.

To measure a hysteresis loop with the rig, the shaker excites substructure A with a harmonic oscillation, leading to a relative motion between the specimens A and B. Either F_{ex} or the relative motion of the specimens, Δx , can be controlled during the excitation. Two single point Laser-Doppler-Vibrometers (LDVs) are focused on the two specimens close to the contact interface (less than 1 mm away as in Fig. 2c) and measure the tangential relative motion. Such a close position to the contact provides accurate displacement measurements without large influences from the bulk material deformation. The LDVs (Polytec OFV-503) record velocity data (velocity decoder) that is integrated in the time domain using trapezoidal integration to obtain the relative displacement $\Delta x = x_A - x_B$. The three load cells measure the T that is transmitted at the contact. The sum of their signals gives the full transmitted force. Plotting T against Δx results in a hysteresis loop. An example is shown in Fig. 3.

A typical hysteresis loop with gross slip shows three distinct stages: (① – ②, ④ – ⑤) stick regime, (② – ③, ⑤ – ⑥) microslip and (③ – ④, ⑥ – ①) gross slip. In the stick regime, Δx originates fully from the elastic deformation of the asperities at the contact interface resulting in a linear dependency between T and Δx . This relationship is described via the tangential contact stiffness k_T . As T increases, some of the contacting asperities start to slide while others are still sticking. This phase is called microslip. When all asperities in contact start to slide, the gross slip state is reached, and T becomes equal to the friction limit μN , where μ is the friction coefficient and N is the normal load. The area within the loop represents the dissipated energy during one cycle and is responsible for the friction damping of the structure. If gross slip occurs, another stiffness can be extracted from the hysteresis loop: the equivalent stiffness k_{eq} which is the average slope of the full hysteresis loop as sketched in Fig. 3. k_{eq} describes the non-linear hysteresis loop by a linear function, leading to an average stiffness that the assembled structure experiences during vibration [9]. When hysteresis loops are in a fully stuck condition, i.e. no slip occurs, k_T and k_{eq} coincide. Although hysteresis loops are a function of T and Δx , the different stages are dependent on the ratio of N and F_{ex} , which are the variables to be controlled in measurements. Please note that F_{ex} is linked to T via the structure's properties, thus they are not identical but F_{ex} has a strong influence on T .

As previously mentioned, FBS assumes linear(ized) and time-invariant structures which are in a steady-state. Thus, in this study, only hysteresis loops that are in a fully stuck condition (and thus show linear behavior) are investigated, with the goal of determining the tangential contact stiffness k_T of the contact.

For the interpretation of the measurements in this study, the first eigenmode of the rig is of importance. This mode is mainly characterized by a horizontal movement of the rig, which corresponds to the sliding direction of the specimens. Previous studies on the rig [9,39] showed that the mode's natural frequency changes when the N and F_{ex} is changed. When the interface is in fully stuck condition the first eigenfrequency of the rig is at 208 Hz. Once gross slip initiates, this eigenfrequency decreases (as far as to 40 Hz) due to a softening of the joint. This behavior shows that the first eigenfrequency is strongly influenced by the properties of the joint and thus, can give important information on contact properties, e.g. such as if the interface is in fully stick condition.

3.2. Dynamic substructuring measurements

A test campaign using single impacts was conducted to investigate the FBS approach. This campaign included measurements on the assembly as well as on both uncoupled substructures. During these measurements the shaker was detached from the substructure A. The measurements on the assembly were conducted while applying a high normal load of 300 N, which could not be applied when measuring the uncoupled substructures, and a impact force for the hammer F_{imp} of 50 N, which was kept the same for the whole impact test campaign. The low ratio of F_{imp} to N made it possible to be in a linear, fully stuck condition at the interface. To measure the admittance of the uncoupled substructures, substructure A's arm needed to be supported since it could not rest on the lower arm B. For that, a vinyl-wire (diameter of 1 mm) was used as seen in Fig. 4b. When substructure A was measured, specimen B was removed to avoid contact between the two specimens and vice-versa.

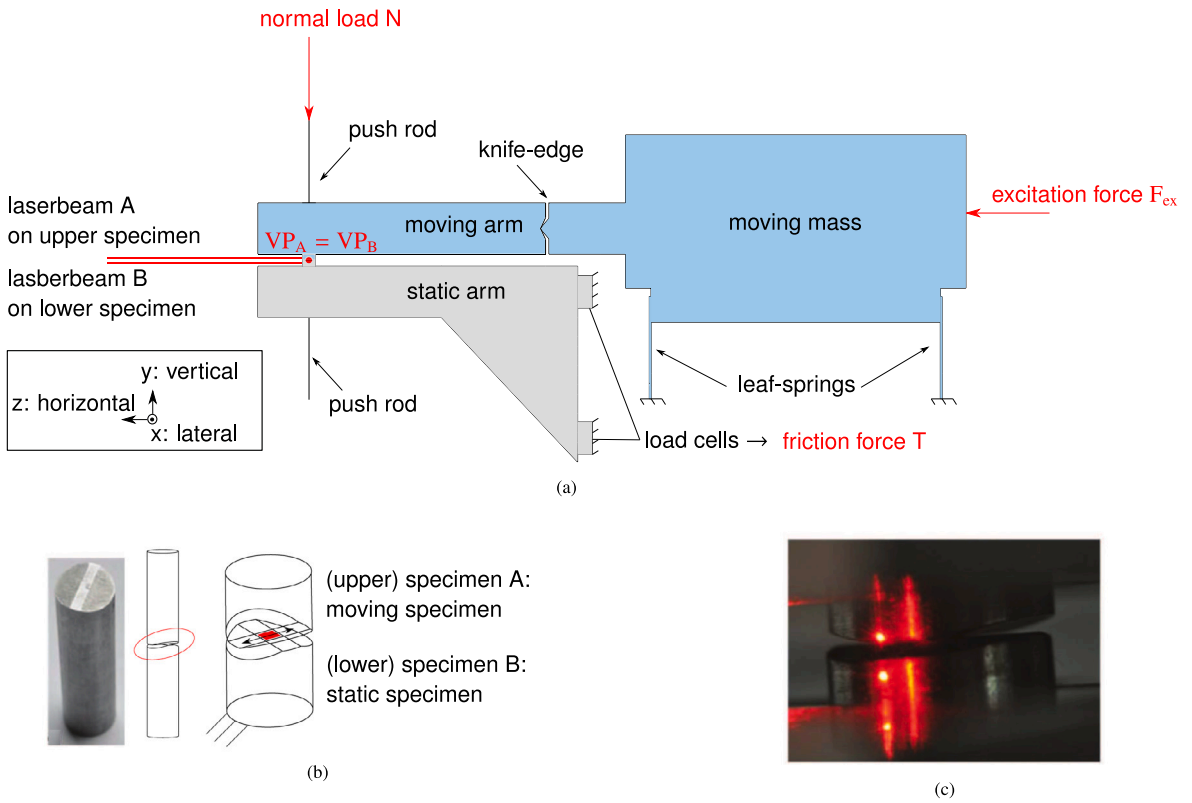


Fig. 2. Friction rig (of Imperial College London) used for this study: (a) schematic figure of the friction rig (b) specimen arrangement for the flat-on-flat contact (c) specimens' contact close view with laser points.

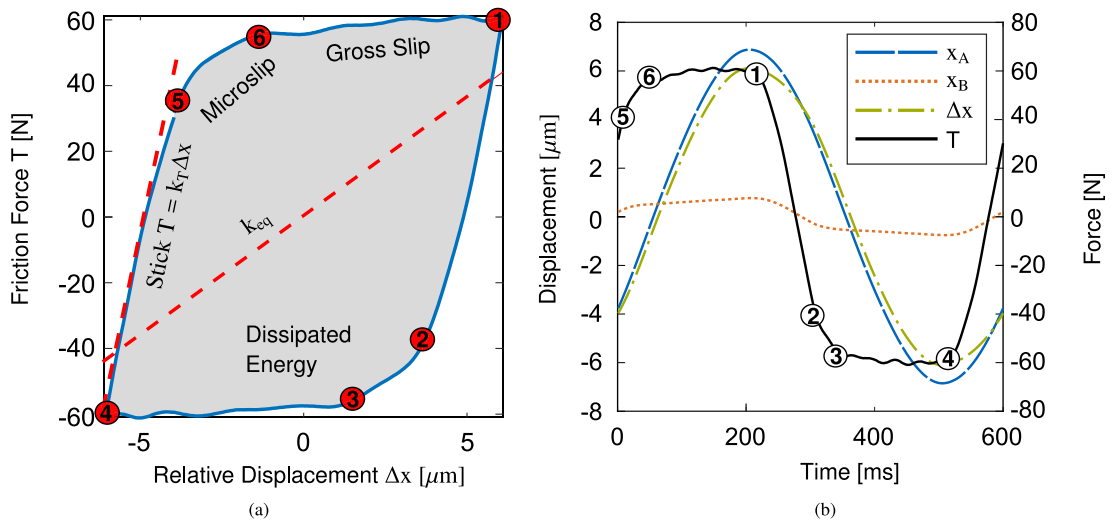


Fig. 3. (a) Typical hysteresis loop with (b) corresponding time signals. From the loop two different types of stiffness can be extracted: The tangential contact stiffness k_T , which is the slope of the stick regime, and the equivalent contact stiffness k_{eq} , which is the average slope of the full hysteresis loop when gross slip occurs.

Due to the inaccessibility of the interface of the specimens to conduct impacts or response measurements, a virtual point transformation (VPT) [26] with two matching virtual points (VPs) was used. The VPT is a reduction process that transforms the measured data from certain locations into one or more VPs chosen by the user positioned in another location, usually close to inaccessible measurement points. The reduction process is performed by using a transformation matrix that contains assumed

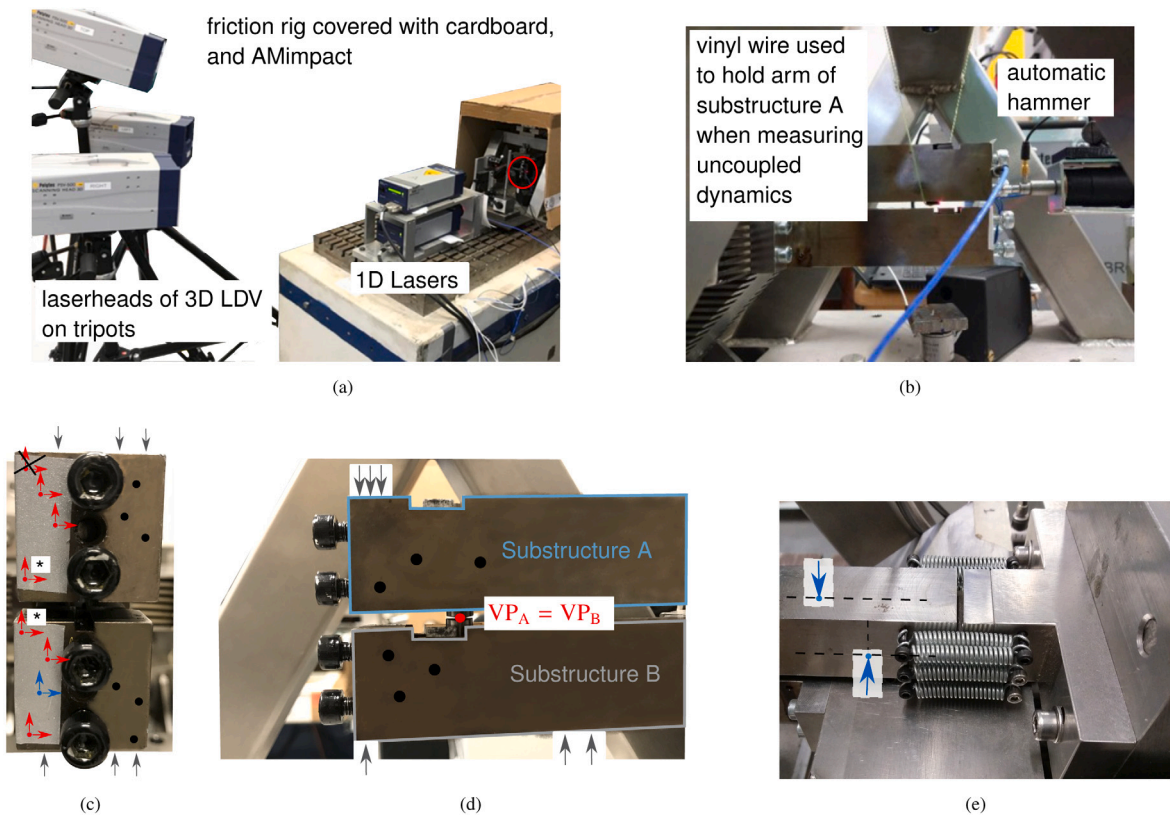


Fig. 4. Photos of measurement set-up and measurement positions: (a) Measurement set-up with 3D scanning vibrometer. The front sides of the friction rig's arms are red circled. (b) Measuring admittances of uncoupled substructures: A vinyl-wire was used to hold the arm of substructure A and avoid contact between the two specimens. (c), (d) Measurement locations on front and side views of the friction rig. The responses were measured on the retro-reflective tape and their positions are marked with 3-dim arrows. The impact locations are marked as black dots in the view planes and arrows in the vertical plane. The black crossed out response locations on substructure A was not used for the VPT due to noise pollution. The blue colored response location marks the internal DoF of substructure B that was not used for the VPT. Additionally the position of the VPs is visualized. (e) Close view knife edge with internal impact DoFs in the two spatial directions x and y , marked as blue arrows. The third internal DoF (z -direction) was conducted on the backside of the moving mass, close to the shaker attachment point and is not visualized here.

deformation shapes of the interface region. In this study, the position of the VPs has been chosen such that they sit on the interface of the two specimens and have the same coordinates. However, their motion is described from different data sets. Only data measured on the substructure A, whether obtained from the part alone or from the assembly configuration, were transformed onto VP A and only data obtained from substructure B (either individual part or assembly) were transformed onto VP B. In this way, the two VPs can still have a relative motion, which results in a finite contact stiffness.

The VPT requires an overdetermined system and Van Der Seijs [26] suggested measuring, for each VP, the three-dimensional translational response at a minimum of three locations and conducting at least three impacts per spatial direction x , y and, z sufficiently close to the interface. In this study, responses were measured on four different locations to provide more data for post-processing but only three locations were used for the VPT. One response location (black crossed out in Fig. 4c) on substructure A was not used for the VPT since the data was too noise polluted and one response location (blue colored 3-dim arrow in Fig. 4c) on substructure B was used as internal DoF and thus also not used for the VPT. Impacts were performed on 9 different positions per substructure as shown in Fig. 4 and described in Table 1. Additionally, three impacts on internal DoFs were conducted on Substructure A. All measurement positions were maintained in the same locations on the individual substructures and the assembly to minimize bias errors. The vibration measurements were performed with a 3D Scanning Laser Doppler Vibrometer (3D SLDV) from Polytec (PSV-500-3D-HV-Xtra) capable of measuring responses simultaneously in all three spatial directions per measurement point. A reflective tape was used to improve the signal quality. The LDV measurement has the advantage of being contactless, eliminating additional mass loading due to the sensors. Furthermore, the LDV allows a precise determination of the measurement location, while for other sensors, such as accelerometers, the true location of the sensing is somewhere within its housing, which is a serious uncertainty when applying a VPT. However, measuring with LDVs comes with the challenge of maintaining the same measurement position for the assembly and then for the individual substructures, while accelerometers do not present this shortcoming since they can be glued to the structures, thus being in the same position for all measurements. In addition, the positions of the three laser beams needed to be calibrated for each structure separately to obtain accurate results and reduce measurement noise. All measurement conditions and equipment are listed in Table 1. Fig. 4 shows the measurement set-up and measurement positions.

Table 1
Measurement conditions and equipment.

Measurement equipment	3D Scanning Laser Doppler Vibrometer by Polytec (PSV-500-3D-HV-Xtra) with acquisition system (decoder DV-08).
Excitation source	Automatic hammer AMImpact [40], to increase repeatability of impact strength and impact position. The impact force was chosen to be 50 N.
Normal load	300 N, close to the maximum achievable normal load to assure a stick condition.
Resolution	Highest possible time resolution that could be handled with the acquisition system to catch peak of impact and to assure best possible repeatability. Frequency resolution 0.5 Hz.
Impact positions	9 per substructure A and B, including 3 per spatial direction x, y, z around the contact interface to obtain an over-determined system for the VPT. Care was taken to excite all 6 DoFs of the VP. Additional 3 impacts on substructure A used as internal DoFs.
Averaging	Needed to reduce measurement noise. After transferring the time data to the frequency domain and eliminating poor quality data (noise polluted, double impacts) 5–8 impacts per response location remained for averaging.
Response locations	Four per substructure A and B to get an overdetermined system. Each response location includes information on x, y, and z-direction.
Cardboard enclosure	Needed to protect the rig from the environmental lights to improve the signal of the range finder laser that is used for the calibration of the laser beams. The accuracy of the calibration has a very high influence on the quality of the measurement results. The responses itself are measured with non-visible infrared lasers.

Signal processing:

The acquisition system of the PSV-500-3D-HV-Xtra was used to record and store time-data, which were then used for further processing. In total, the time signals (2 s each) of 2016 impacts were measured. A rectangular window was applied to all force signals (impulse) and an exponential window to the response signals (decaying signal) to minimize leakage [41]. A Fast Fourier Transformation (FFT) was applied to the windowed time data to obtain the frequency information. Noise polluted or double impact data was removed at this stage. Afterwards, the cross-power spectrum and auto-power spectrum were calculated and a minimum of 5 impacts averaged to reduce measurement noise. From the resulting data set, Frequency Response Functions (FRFs) were calculated via H1-estimator [41]. Only data up to 2000 Hz was considered at this stage since this frequency range could be excited properly by the used vinyl hammer tip. This frequency range was chosen by looking at the input power spectrum and considering only data before a drop of -6 dB. The obtained FRFs were then used for post-processing.

Post-processing:

As previously mentioned, a VPT was used to represent the interface motion without measuring it directly. The VPT is a reduction process that transforms the measured data onto the VPs with the use of a transformation matrix that includes possible Interface Deformation Modes (IDMs). Each VP has as many DoFs as IDMs are used for the transformation, e.g. 2 IDMs lead to 2 DoFs per VP. The IDMs describe the possible (reduced) motion of the joint. It is important to accurately identify which IDMs are needed, and how many, to describe the joint in the best way. A complex mode indicator function (CMIF), based on a Singular Value Decomposition (SVD), of the measurement data was performed to gain important information on the number and possibly motions of the significant IDMs. The Appendix B describes this procedure in more detail. In this study, three different sets of IDMs are compared to show their influence on the results. The comparison of the IDMs can also help to identify if possible discrepancies in the extracted contact stiffness values are an IDM issue or a FBS approach issue. If only one IDM case leads to significant different results, it is likely due to an IDM issue, e.g. insufficient description of the joint. Based on the CMIF, only rigid body modes were used as IDMs and thus, it was assumed that the joint behaves rigidly. The investigated IDMs are the following:

- 2 IDMs: The CMIF study in the Appendix B suggests 2 IDMs as a minimum number of DoFs to describe the joint. Here, two translation modes (horizontal and vertical) were chosen since they were extracted from the singular vectors of the CMIF and assumed to best describe the first eigenmode of the friction rig, which is a combination of a movement in horizontal direction and bending/rotation of the arms.
- 4 IDMs: Two translations (horizontal and vertical) and two rotations (around the lateral and vertical axis, see Fig. 2a for specification).
- 6 IDMs that give the full set of rigid body modes (i.e. three translations and three rotations).

For each IDM case, contact stiffness values were extracted from the dynamic stiffness matrix of the joint $Z^{(J)}$. The real part of $Z^{(J)}$ represents only the stiffness $K^{(J)}$, see Eq. (2), since the joint is assumed to be massless as it is realized only by contact of parts that are fully included in the two substructures without any additional parts, e.g. screws or rubber mounts. Each diagonal element of $K^{(J)}$ contains the stiffness between a pair of coupled DoFs across the interface. Here, the DoFs that represent the stiffness in the z-direction (i.e. horizontal motion), $k_z^{(J)}$, correspond to the tangential contact stiffness.

Despite a measured frequency range up to 2000 Hz, data only up to 800 Hz is included in the analysis because the range above 800 Hz is affected by a coupling of the substructures through the leaf springs. The leaf springs connect the moving mass of substructure A to the ground, to which also the force transducers of substructure B are connected (see Fig. 2a). Investigations

showed that, below 800 Hz, the transmission of signals through the leaf springs is negligible while, above 800 Hz, results of FBS approaches might be affected by a back-coupling of signals through the leaf springs. Since the decoupling methods described in this paper assume that the substructures A and B are uncoupled if the joint under investigation is not present, the frequencies above 800 Hz were not used for stiffness value extraction. The first 100 Hz were also neglected as they are polluted by measurement noise. The reason for this high noise effect at low frequencies is investigated in the [Appendix C](#).

3.3. Hysteresis loop measurements

Hysteresis loops were obtained in two ways: (1) with shaker tests (traditional rig configuration) and (2) with impact tests. The shaker tests were performed before and after the FBS campaign to assess if the contact conditions changed during the FBS campaign. The impact tests were part of the FBS campaign itself, and therefore hysteresis loops from the impact tests were extracted simultaneously with the data used for FBS. The applied normal load during these measurements was kept constant at a high value of 300 N to ensure a stick condition of the interface. Contact stiffness values were extracted from the hysteresis loops by fitting a line via least square and using its slope as the contact stiffness value.

Shaker test:

During the shaker tests, the specimens' relative displacement amplitude, Δx , was controlled. Three different levels were excited: $\pm 0.1 \mu\text{m}$, $\pm 0.15 \mu\text{m}$, and $\pm 0.2 \mu\text{m}$, to investigate the influence of the Δx on the results and allow a comparison with the impact test campaign, whose displacement amplitudes were in the same order of magnitude. For each displacement amplitude level, five different frequencies were excited to investigate the variation of the contact stiffness over the frequency range. The investigated excitation frequencies were the following: 100 Hz, which is known to give high quality hysteresis loops on the studied rig [9]; the 200 Hz, which was chosen as it is close to the first eigenfrequency in stick condition (208 Hz) but stable enough to be controllable, and then, moving away from resonance, 250 Hz, 300 Hz and 500 Hz to get a range of excitation frequencies.

Impact test:

During the impact test campaign for the FBS approaches, the friction force and relative displacement, required for the hysteresis loops, were recorded by saving the decaying time signals of the three load cells, and the two 1D lasers. Here, only data with excitation in horizontal direction (z -direction) was used in order to obtain the tangential contact stiffness. Two types of impact positions were investigated: an impact position on the backside of the moving mass, close to the location where the shaker would excite the structure in the "standard rig configuration", and the three impact positions on the front-side of the moving arm (see [Fig. 4c](#)). This is done to investigate if the impact location has a significant influence on the hysteresis loop results, which is also important for further comparison with the FBS measurements. Please note that hysteresis loops resulting from impacts on the static arm cannot be used for comparison with the shaker test and FBS since the force measured by the load cells is no longer solely the transmitted friction force through the specimens.

4. Results of hysteresis loop measurements — time domain experiments

This section presents the contact stiffness determination obtained from the two types of hysteresis loop measurements, shaker test and impact test, described in [Section 3.3](#).

4.1. Hysteresis loop measurements from shaker tests

[Fig. 5](#) shows the mean stiffness values and their standard deviations that were extracted from the hysteresis loops recorded during the shaker tests. Three different relative amplitudes Δx of the specimens for five different excitation frequencies are plotted. Only the smallest Δx could be measured at 500 Hz excitation frequency due to shaker limitations. The measurements were conducted before and after the impact test campaign to assess if the contact conditions changed due to the impact test campaign. The main observations are:

- The larger the Δx the lower the k_T . This trend was observed in previous studies [42–44] and is thought to be due to reduced junction growth and aging at the interface at large relative displacement [19].
- The extracted contact stiffness values, before and after hammer testing, are very repeatable for higher frequency tests, meaning that the impact test campaign did not change significantly the contact properties of the interface. However, at 100 Hz, a larger scatter is observable. The reasons for this are not fully understood yet. They might be due to some interactions between the interface properties and the system dynamics that are only activated at 100 Hz.
- The obtained stiffness drops slightly from 100 Hz to 200 Hz, but then increases significantly at 250 Hz. After 250 Hz, the contact stiffness value increases only slightly with the excitation frequency.

To better investigate the drop in the contact stiffness at 200 Hz, the time signals of the hysteresis loops were studied in more detail. It was found that the drop in stiffness is caused by excitation of a rig resonance that introduces a phase shift between the two specimens. [Fig. 6](#) shows three exemplary loops and their corresponding time signals, which are plotted in the sub-figures below the loops. The time signals show the displacements of the specimens, x_A and x_B , the resulting relative displacement Δx , the harmonic excitation force from the shaker applied to substructure A, F_{ex} , and the transmitted friction force through the specimens' contact interface, T , that is measured by the three load cells of substructure B. The hysteresis loops were measured at 100 Hz, 200 Hz,

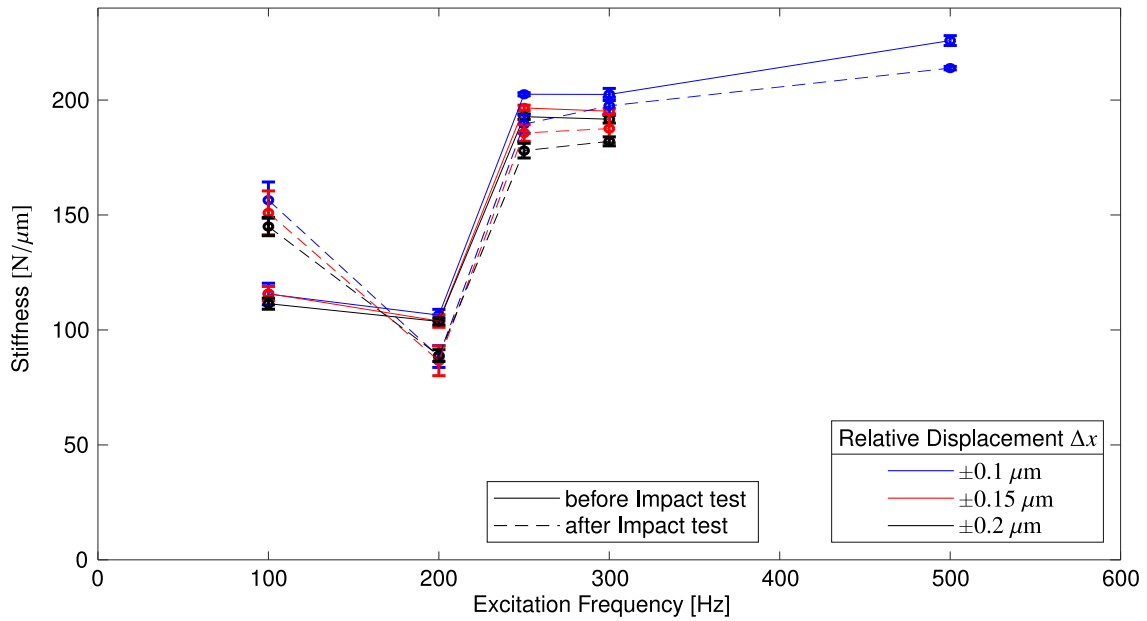


Fig. 5. Contact stiffness values extracted from hysteresis loop measurements with shaker excitation and their standard deviation as error bars. Experiments were performed before and after the impact test campaign for different excitation frequencies and Δx at a constant normal load of 300 N.

and 250 Hz respectively for a Δx of $\pm 0.15 \mu\text{m}$. Note that the first eigenfrequency of the system is at 208 Hz and therefore the 100 Hz loop was measured before resonance, the 200 Hz loop close to resonance, and the 250 Hz loop after resonance. No loops were measured at the rig's first eigenfrequency at 208 Hz, because it was challenging to control the relative displacement Δx at resonance. Fig. 6 shows that the displacement of specimen B, x_B , is always in phase with T . This indicates that specimen B and the static arm are effectively a rigid body, as expected, and hence the clamping of specimen B to the static arm does not introduce any lag in the response. Fig. 6d shows that before resonance, at 100 Hz, displacements (x_A and x_B) and forces (F_{ex} and T) are in phase. After the resonance frequency, at 250 Hz, (Fig. 6f) the excitation force F_{ex} and the response signals have a phase shift of 180 degree, indicating the expected transition beyond a rig resonance. Notably, the hysteresis loops that were measured before and after resonance are in fully stick condition (linear line in Figs. 6a and 6c), but the loop that was measured close to resonance, 200 Hz, (Fig. 6b) is elliptically shaped. The corresponding time signals of the 200 Hz excitation in Fig. 6e show that x_A and x_B are no longer in phase, leading to a phase shift in the resulting Δx . Consequently, Δx and T have a phase difference, which results in an elliptical hysteresis loop. This elliptical orbit explains why the contact stiffness of the 200 Hz case drops in Fig. 5. Here, the linear fit no longer provides a k_T estimation, but rather a k_{eq} that has a lower value (see Fig. 6b) as it has a smaller slope. Note, that the elliptical shape is not an indicator for a sliding interface because (i) a sliding interface shows the shape of non-symmetric rectangle instead of a symmetric ellipse, and (ii) during the measurements the Δx was controlled at a very low value where gross slip is very unlikely. Additionally, it is to be noted that x_A is lagging behind x_B , which is somewhat unexpected since specimen B is excited by specimen A. These aspects needed further investigation and possible answers are given in the following section.

4.2. Hysteresis loop measurements from impact tests

This section investigates the hysteresis loops recorded during the FBS impact campaign and compares them to the results from the shaker test in Section 4.1. Before showing the results, the main difference between the shaker test and the impact test, as they were conducted in this study, needs to be highlighted: the shaker excited one certain frequency at a time with a constant displacement amplitude, while the hammer impact (impulse signal) excited a frequency range with corresponding decaying time signals. Therefore, in the case of impact tests, all excited frequencies are present in the first cycle of the decaying time signals, while the higher frequencies damp out fast and only the lower ones remain. The therefrom estimated stiffness values cannot directly be linked to a distinct excitation frequency.

Fig. 7a shows an example of the time response signals obtained from an impact conducted on the front side of the moving arm. From the time signals in Fig. 7a, it was determined that the main frequency content of T and x_B was 208 Hz, which is the first eigenfrequency of the rig with a fully stuck interface as described in Section 3.1. This is important as it proves that the specimen interfaces were not in gross slip. In the first cycle, from roughly 0 s to 0.005 s, displacement and force signals are in phase and the corresponding loops are in stick condition, see Fig. 7b. Higher frequency contents are clearly visible in the shape of the loop, which does not show a single straight line but a wobbling signal in line shape. The estimated k_T values of the stick loops have a mean value of 180 N/ μm with a standard deviation of 6 N/ μm for a Δx of approx. 0.15 μm and are in agreement with the k_T extracted at

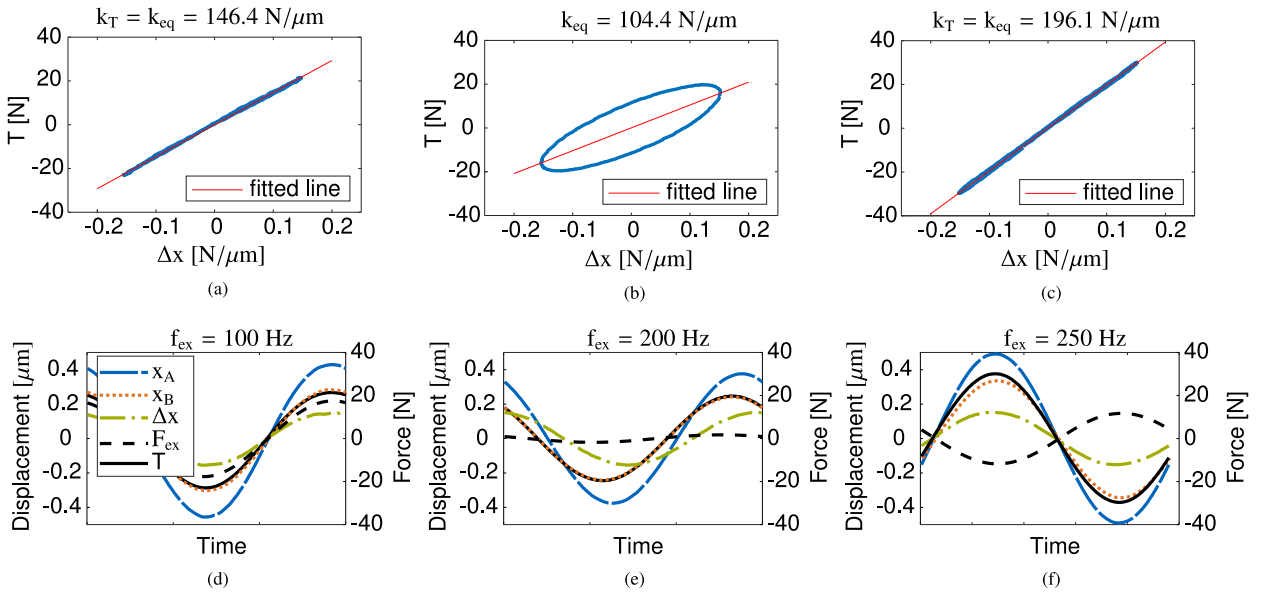


Fig. 6. Time signals and the resulting hysteresis loops for a Δx of $\pm 0.15 \mu\text{m}$ for three different excitation frequencies (measured after the impact test campaign): (a), (d) before resonance; (b), (e) close to resonance; (c) and (f) after resonance. The hysteresis loops before and after resonance show a stick stage from which a $k_{eq} = k_T$ can be extracted, while the hysteresis loop close to resonance is elliptically shaped and only a $k_{eq} \neq k_T$ can be determined. The legend for the time signals is only shown in (d) for clarity but also valid for (e) and (f).

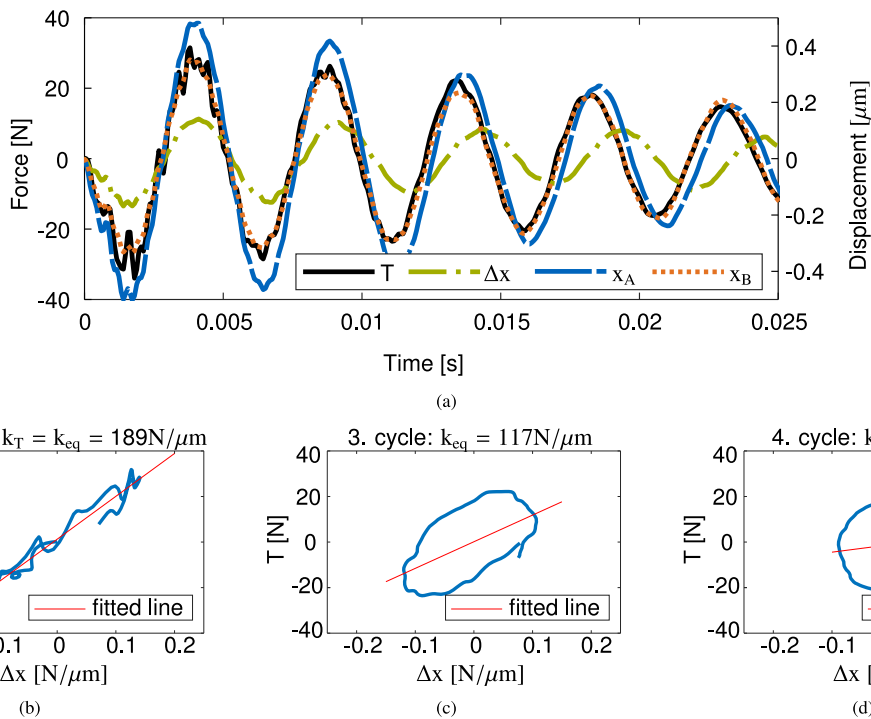


Fig. 7. Time signals and hysteresis loops from the impact test campaign: (a) Time signals - impact excitation on moving arm (b) hysteresis loop of first cycle (c) hysteresis loop of 3rd cycle (d) hysteresis loops of 4th cycle.

250 Hz and above during the shaker tests in Fig. 5. When the excitation impulse is applied on the moving mass (where the shaker excites the structure in shaker tests) and not on the moving arm, the results are similar and thus, not shown here.

Fig. 7a shows that, after the first cycle, T and Δx start to go out of phase, with consequences on the extracted stiffness value. In fact, as soon as there is a phase difference between T and Δx , the corresponding loops become elliptical, and, thus, a k_{eq} results from

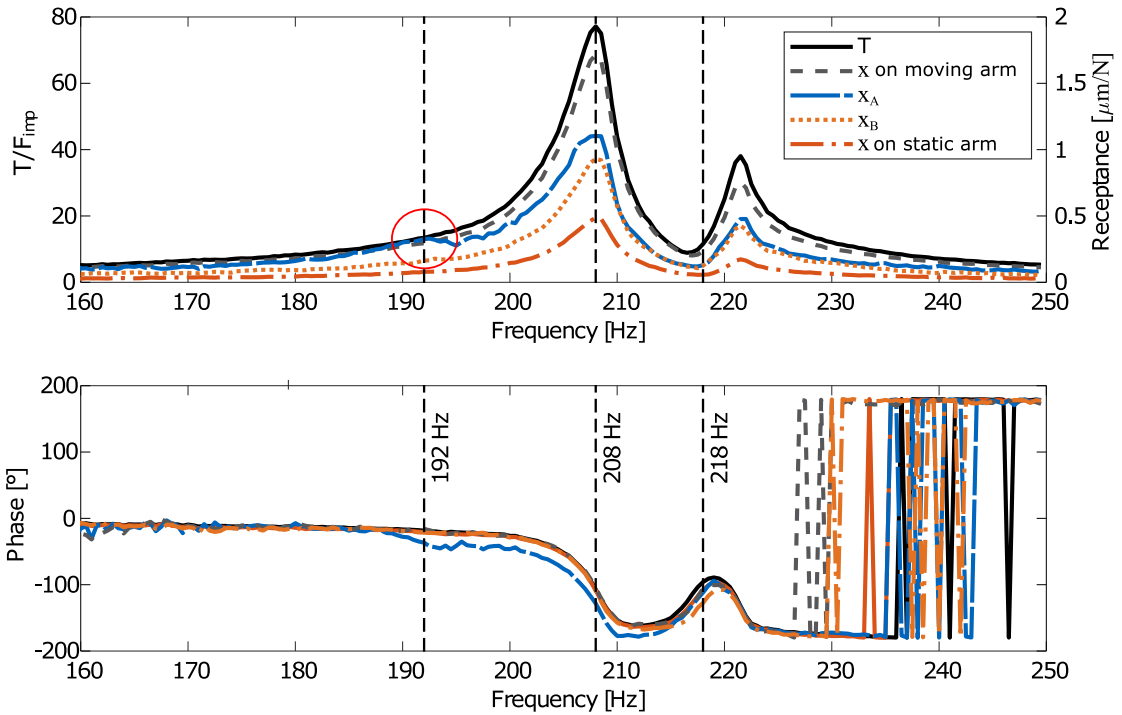


Fig. 8. FRF investigation: A local resonance in the signal x_A of specimen A is visible (red-circled) and causes an out-of-phase motion of the two specimens.

a linear fitting and not a k_T representative of the contact interface. Examples are shown in Figs. 7c and 7d. This effect has already been observed in the hysteresis loop of the shaker test with 200 Hz excitation frequency (see Fig. 6b). The k_{eq} values are dependent on the phase difference of T and Δx . The higher the phase difference, the lower the obtained k_{eq} . From Fig. 7a it is shown that the phase difference changes with progressing time. It was verified that this behavior does not occur due to the time integration of the velocity data.

In 4.1 it is stated that the elliptical loops appear at excitation close to the rig’s first eigenfrequency. However, Fig. 8 shows that the reason for the phase difference between the specimens, and hence the elliptical hysteresis loops, is due to the activation of a local resonance of specimen A. The Figure plots the FRFs obtained from the decaying time response signals x_A , x_B and T , and from signals of the moving arm and the static arm measured by the 3D LDV (for the substructuring analyses) within the assembly configuration. The response signals on the arms were obtained from the locations marked with a * in Fig. 4c. A hammer impact conducted on the back-side of the moving mass was used as reference. Notably, a small peak and phase jump are present in the signal of specimen A at 192 Hz, while they are not present in the other signals. Since the small peak (red circled in Fig. 8) only appears in the signal measured directly on specimen A, this resonance is most likely due to the clamping mechanism of the specimen. Further investigations showed that this peak in the signal of specimen A appears only in the assembly configuration and not when the substructure A is measured alone. This indicates that this local resonance of specimen A is activated through the applied normal load and interaction with substructure B. The phase plot in Fig. 8 shows that, due to this local resonance, the signal of specimen A goes out of phase with the other signals before retrieving a common phase again at around 218 Hz.

A mathematical reconstruction of the time signals is shown in Fig. 9. The reconstruction was performed by extracting the magnitudes from the FFT of x_A at 192 Hz and 208 Hz and from the FFT of x_B at 208 Hz and generating sinusoids. This plot supports the fact that, due to the resonance at 192 Hz, specimen A goes out-of-phase with specimen B and the rest of the structure and starts lagging behind. Consequently, this local resonance causes the out-of-phase movement of the two specimens resulting in the observed elliptical hysteresis loops, obtained from either impact and shaker tests.

4.3. Summary hysteresis loop measurements

In this section, hysteresis loops obtained from shaker tests and from impact tests are compared. The shaker tests were performed at five distinct harmonic excitations (100 Hz, 200 Hz, 250 Hz, 300 Hz, 500 Hz) while, during the impact tests, a frequency range of up to 2000 Hz was excited through the impulse excitation. During the tests, care was taken to maintain fully stuck conditions and avoid gross slip of the specimens by keeping a very large normal load and very low tangential excitations.

It was observed that contact stiffness values extracted from fully stuck hysteresis loops strongly depend on the excitation frequency. When the excitation frequency was close to the first eigenfrequency of the friction rig, which is at 208 Hz, the shape

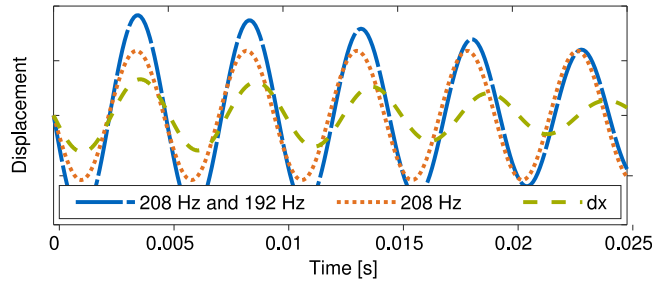


Fig. 9. Reconstruction of the measured time signals presented in Fig. 7a.

Table 2

FBS contact stiffness estimations: mean values and standard deviations.

Frequency range	300 Hz – 600 Hz	100 Hz – 800 Hz
2 IDMs	$k_{z,mean}^{(J)} = 52 \text{ N}/\mu\text{m}, \sigma = 10 \text{ N}/\mu\text{m}$	$k_{z,mean}^{(J)} = 32 \text{ N}/\mu\text{m}, \sigma = 40 \text{ N}/\mu\text{m}$
4 IDMs	$k_{z,mean}^{(J)} = 26 \text{ N}/\mu\text{m}, \sigma = 10 \text{ N}/\mu\text{m}$	$k_{z,mean}^{(J)} = 22 \text{ N}/\mu\text{m}, \sigma = 23 \text{ N}/\mu\text{m}$
6 IDMs	$k_{z,mean}^{(J)} = 27 \text{ N}/\mu\text{m}, \sigma = 4 \text{ N}/\mu\text{m}$	$k_{z,mean}^{(J)} = 27 \text{ N}/\mu\text{m}, \sigma = 56 \text{ N}/\mu\text{m}$

of the hysteresis loops became elliptically shaped and, thus, the estimated stiffness value k_{eq} was lower than the k_T . Investigations showed that the elliptically loops resulted from a phase lag between the displacement signals of the two specimens, which results in a phase difference of Δx and T . A local resonance of the clamp of specimen A caused this phase lag, which was identified with a FRF investigation of the decaying time signals obtained from impact tests. The local resonance of the clamp at 192 Hz was activated only in the assembly configuration and spread its influence over a wider frequency range, as seen from the phase plot in Fig. 8.

These results show that local joint resonances can strongly influence the extracted contact stiffness value, even over a wide frequency range, and that fully stuck hysteresis loops can indicate such hidden resonances by becoming elliptically shaped. These loops are not true hysteresis of the contact, which indicate gross slip, but an artifact coming from the phase lag of the specimens. In this case, the interface is still in stick condition but the measured Δx is not representative for the actual Δx exhibited at the contact interface. This is because x_A and x_B are not measured at the contact interface directly but few tens of millimeters far from it, as shown in Fig. 2c. As a result, part of the measured displacement is due to some tilting of the specimen A probably induced by its resonance clamping vibration. Therefore, the estimated stiffness is not the true contact stiffness of the interface, but is an equivalent stiffness resulting from the elliptical hysteresis loop due the dynamics close to the contact.

This aspect must be considered when hysteresis loop measurements are needed to provide input contact parameters for contact models. High-frequency vibrations might in fact activate unexpected local joint resonances that lead to misleading displacement measurements with consequent misleading contact stiffness estimations. This described shortcoming was unexpected since it is commonly assumed that contact parameters extracted from low amplitude hysteresis loop measurements are not influenced by structural resonances, but only by features such as displacement amplitude, material pair, normal load, temperature etc.

5. Results of substructuring measurements — frequency domain experiments

This section describes the results of the FBS measurement campaign, which was performed on the friction rig to obtain the tangential contact stiffness to be compared with hysteresis loop measurements. Four different approaches were investigated but only the approach that provided the cleanest results, i.e. the *decoupling interface and internal DoFs*, is presented here. The results of the other approaches are shown in the Appendix A. In this approach, internal DoFs are used for decoupling in addition to interface DoFs. The used internal DoFs are the blue-colored impact and response locations in Fig. 4c-e.

The resulting $k_z^{(J)}$, one for each Interface Deformation Mode (IDM) case, are plotted in Fig. 10. The graphs show a linear, almost constant, trend with frequency thus suggesting that the contact stiffness extracted from FBS is independent of the frequency. A signal quality variation is present over the investigated frequency range, which is attributed to measurement uncertainties and uncertainty propagation in the joint-identification method used. This quality variation leads to the question of which frequency (range) should be used for the contact stiffness extraction. This is relevant considering that hysteresis loops (from shaker tests in standard rig configuration) are measured at distinct excitation frequencies and therefore provide stiffness values at these distinct frequencies. Instead, the investigated FBS approaches hardly allow to do so and, therefore, it was decided to extract stiffness values over two different frequency ranges: 300 Hz – 600 Hz and 100 Hz – 800 Hz. The first range was chosen because it is narrow enough to provide more accurate and less noise polluted estimations. The second frequency range consists of the whole considered frequency range. It was decided to take the mean value of each investigated case as the FBS contact stiffness estimation, $k_{z,mean}^{(J)}$. The mean $k_{z,mean}^{(J)}$ over these spectrums and their standard deviations are listed in Table 2, which shows that the influence of the different IDMs on the $k_{z,mean}^{(J)}$ is almost negligible.

Since other approaches (see the Appendix A) showed a greater dependency of the results on the IDMs and the *decoupling interface and internal DoFs* is the only investigated method that used internal DoFs, it is concluded that the information from the here

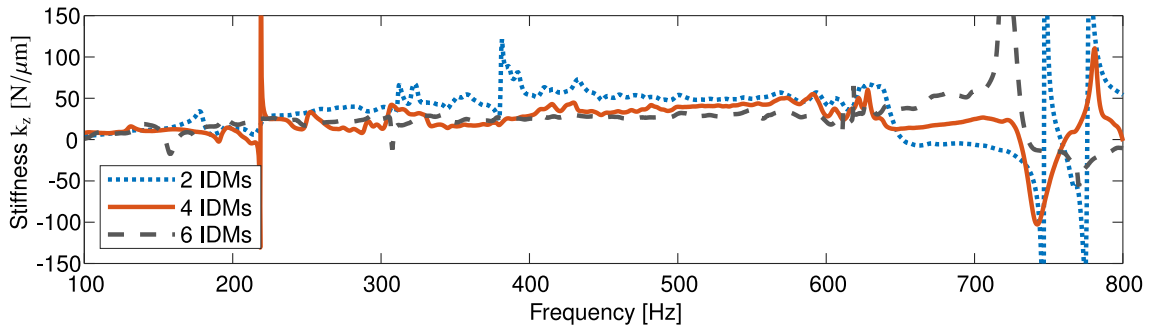


Fig. 10. Decoupling with interface and internal DoFs.

Table 3
Hysteresis loop contact stiffness estimations: mean values and standard deviations.

Shaker test	Impact test
k_T from 250 Hz, 300 Hz	k_T from first cycle, all excited frequencies
$\Delta x = 0.15 \mu\text{m}$:	$\Delta x = 0.15 \mu\text{m}$:
187 N/ μm , $\sigma = 5 \text{ N}/\mu\text{m}$	180 N/ μm , $\sigma = 6 \text{ N}/\mu\text{m}$
k_{eq} at 200 Hz,	k_{eq} from subsequent cycles, cannot be linked to a certain frequency
$\Delta x = 0.15 \mu\text{m}$:	Depending on phase difference, e.g. 4th cycle:
86 N/ μm , $\sigma = 6 \text{ N}/\mu\text{m}$	31 N/ μm , $\sigma = 5 \text{ N}/\mu\text{m}$

considered internal DoFs can account for the missing information on the interface when the interface is poorly described through the IDMs, e.g. when using only 2 IDMs. Furthermore, FRFs from internal DoFs are less noisy and thus give important additional information about the structure without adding a lot of additional noise. Thus, this approach provides the cleanest curves if compared to those from the other approaches. The influence of the selected spectrum is reflected mainly in the standard deviation. Here, the σ for the 100 Hz – 800 Hz spectrum shows larger values, which is expected as σ is also a measure of the inherent noise.

6. Comparison and discussion of results: Hysteresis loop measurements and FBS

This section shows a final comparison between the extracted contact stiffness values, k_T and k_{eq} , from local contact hysteresis loop measurements presented in Section 4 and the extracted $k_{z,mean}^{(J)}$ values from the global dynamics investigation of the friction rig via the FBS approach of Section 5. It is investigated if FBS can be used to extract the tangential contact stiffness and how the vibration behavior of structures is related to their contact properties. Table 2 shows a summary of the FBS results and Table 3 a summary of the hysteresis results.

With regards to the hysteresis measurements, the contact stiffness k_T was estimated from stick hysteresis loops and represented the rigid joint stiffness. It is the highest determined stiffness. The equivalent stiffness k_{eq} was instead lower and was obtained from elliptical shaped hysteresis loops that originated from the influence of a local joint resonance. The comparison of Tables 2 and 3 shows that the $k_{z,mean}^{(J)}$ values extracted from FBS approaches are far lower than the k_T and closer to the k_{eq} values found with hysteresis loop measurements. A possible explanation is that the VPT of the FBS approach, as it was applied in this study, assumed that the structure between the measurement locations and the VPs was rigid. However, the 192 Hz resonance of the clamp contradicts this assumption, which is not valid along the whole investigated frequency range. Furthermore, the applied decoupling approach can only eliminate the behavior of the substructures, but not behaviors that appear due to the joint. Decoupling is basically $AJB - A - B = J$, with A and B as substructures, J as joint and AJB as assembly. Although the joint is massless, J stores all the difference between the assembly and the substructures and thus all the dynamics of the joint. This means that, besides eliminating the influence of the substructures in the assembly, the resulting joint has not only contact properties but also its own dynamic properties, e.g. the local resonance at 192 Hz due to the clamping that softens the contact stiffness, as described in Section 4.2. It is thus assumed that the k_{eq} and $k_z^{(J)}$ describe the same kind of equivalent contact stiffness, since they both originate from the same phenomenon (clamp resonance). However, this stiffness is not representative of the tangential contact stiffness that instead is a property solely of the contacting interfaces and is characterized by a linear relationship of the friction force with the tangential relative displacement.

Since the local resonance of specimen A is only activated in the assembly configuration due to the applied normal load and interaction with substructure B, an elimination of this dynamic behavior within FBS might have been possible by using a so-called transmission simulator [45,46]. A transmission simulator is generally used to rebuild the interface of the assembly within the substructure configuration thus making it possible to decouple additional dynamic effects. In order to rebuild the interface here, a stiff plate, welded to specimen A, on which a normal load can be applied, might be a solution. This will be investigated in future studies to further validate the presented measurements.

All the previous findings are summarized below to provide insights into the physics of the contact stiffness and into the reliability of the two measurement techniques to extract the k_T .

Physics of the contact stiffness:

- Two kinds of stiffness were determined in this study: (i) the contact stiffness of the stuck interface, k_T , that is the stiffness of the rigid joint and is due to the loading and contact properties and can be transferred to other structures with the same contact conditions. This stiffness is extracted from fully stuck hysteresis loops, i.e. straight lines; (ii) the softer equivalent stiffness, k_{eq} , that includes information on the dynamics of the interface and is a structure-specific property that needs to be determined on the structure of interest itself. This equivalent stiffness is extracted from elliptical hysteresis loops, which are elliptical because of altered motion of the contacting components. This stiffness is also extracted from FBS measurements when the contacting components are not rigid but show a degree of flexibility.
- Given this distinction, which of those stiffnesses should be used in contact models for the nonlinear dynamic analysis of jointed structures? Either can be used depending on the accuracy of the used finite element (FE) models of the jointed assembly. When FE models are modeled in great detail, the tangential contact stiffness, k_T , should be used as input since the dynamic behavior will already be captured by the detailed FE model. Instead, when simplified models are used, e.g. lumped models with only few degrees of freedom, the k_{eq} should be used as input in the contact models. In fact, the k_{eq} would account for the missing dynamics of the simplified few DoF model.

Reliability of hysteresis and FBS measurements for k_T estimations:

- Hysteresis loops from shaker tests can identify accurate tangential contact stiffness values k_T from stick hysteresis loops at specific frequencies. Elliptical shaped hysteresis loops indicate the excitation of a local joint resonance and thus can help to identify hidden resonances. From these loops an equivalent stiffness k_{eq} value is obtained, which is however not the true contact stiffness of the stuck interface.
- Hysteresis loops from impact tests can identify k_T values from the first cycle of the decaying time signals. Furthermore, the data obtained from the impact test has the advantage that an additionally investigation in the frequency domain is possible, which can help to identify important additional properties of the structure. In this study, the local resonance of the clamp could thereby be identified. Unfortunately, the obtained stiffness values cannot be linked to certain frequencies directly.
- FBS struggles with the determination of stiffness values at specific frequencies due to its noise content and provides average stiffness values over wider frequency ranges. In this study, the determined stiffness values included also dynamic joint information and are thus not representative for the actual stick contact stiffness. However, the authors assume that FBS, can be able to identify k_T for structures with a stiffer joint and less own dynamics or by using a transmission simulator.
- Although, FBS measurement campaigns are very time-consuming and need more effort if more DoFs are to be considered, the same set of measurement data can be used for multiple approaches allowing a broad investigation and comparison of results. If a VPT is used, a comparison of different sets of IDMs is suggested since their influence on the results can be significant, especially when they describe the interface insufficiently.
- The results show that both hysteresis loop and FBS contact stiffness estimations can be affected by joint resonances. While hysteresis loop clearly show this effect in the shape of the loop, FBS results do not allow this distinction. For hysteresis loop measurements, it is thus suggested to investigate multiple excitation frequencies and to use only fully stuck loops for k_T estimation and not eventual elliptical loops distorted by local joint resonances. For FBS measurements, it is suggested to validate the results with another method if a VPT is used for complex joints. In fact, local resonances might exist between the measurement positions and the locations of the VPs, thus invalidating the VPT transformation and leading to possible misleading contact stiffness estimations much lower than the k_T of the real contact interface. It is to be noted that the choice of using only rigid body modes as IDMs for the VPT, and thus the rigidity assumption, was based on the CMIF described in the [Appendix B](#). From the CMIF, the local resonance could not be identified.

7. Conclusion

Frequency based substructuring (FBS) is used to determine the tangential contact stiffness k_T of the stuck interface in a friction rig excited under low amplitude vibration. k_T values are compared to those determined from local hysteresis loops measured simultaneously on the rig itself. This novel and simultaneous comparison is performed to improve the physical understanding of the contact stiffness and to assess the reliability of both FBS and hysteresis measurements in the extraction of k_T .

The comparison showed that local (hidden) joint resonances can lead to inaccurate estimations of the contact stiffness with either measurement technique. In the case of hysteresis loops, local joint resonances led to inaccurate measurements of the relative displacement of the contact interfaces. As a result, elliptical hysteresis loops were observed at low vibration amplitudes, instead of the expected linear fully stuck loops. Those hysteresis loops were not representative of the real contact behavior and therefore they led to misleading contact stiffness estimations. In the case of FBS measurements, local joint resonances invalidated the rigid body assumption of the virtual point transformation (VPT). As a result, the k_T extracted with FBS was not representative of the real contact stiffness of the contact. This invalid VPT assumption should be considered when using FBS to obtain information on the contact of jointed structures.

To overcome the measurement problems induced by local (hidden) joint resonances, it is strongly recommended to verify if such local joint resonances exist in the investigated frequency range. They can be recognized by checking if phase shifts exist in the measured displacements of the two contacting components. This check was done in this study by observing unexpected elliptical loops obtained during the low amplitude hysteresis measurements and also by observing sudden phase shifts in the frequency response functions obtained during the FBS measurements.

These findings shine a new light on the reliability of those two measurement techniques to extract accurate k_T values. In addition, an improved understanding of the contact stiffness is also provided since, when local joint resonances are present, the estimated contact stiffnesses are much lower than the real contact stiffness of the contact interface. This aspect has to be taken into account when using such contact stiffness estimations as input in contact models used for the nonlinear dynamic analysis of jointed structures.

CRedit authorship contribution statement

Verena Gimpl: Investigation, Methodology, Writing – original draft, Visualization. **Alfredo Fantetti:** Conceptualization, Supervision, Methodology, Writing – review & editing. **Steven W.B. Klaassen:** Supervision, Writing – review & editing. **Christoph W. Schwingshackl:** Resources, Writing – review & editing, Funding acquisition. **Daniel J. Rixen:** Resources, Writing – review & editing, Supervision, Funding acquisition.

Declaration of competing interest

The authors declare that they have no known competing financial interests or personal relationships that could have appeared to influence the work reported in this paper.

Acknowledgments

A. Fantetti and S. W. B. Klaassen received funding from the European Union’s Horizon 2020 research and innovation program under the Marie Skłodowska-Curie, UK grant agreement No 721865, project acronym “EXPERTISE”.

Appendix A. Comparison of different FBS approaches

For the FBS investigation further three methods were applied. In this section, their theory is shortly described and the results shown and compared.

A.1. Inverse substructuring

The easiest FBS method to implement and the least time-consuming one in terms of measurements, is *Inverse Substructuring*. The advantage with *Inverse Substructuring* is that it requires only measurement on the assembly, while the other discussed FBS methods within this paper require measurements on the assembly and the decoupled substructures. With the assumption that measurements only on the interface DoFs c are performed this approach can be written as in Eq. (A.1).

$$\left(\mathbf{Y}_{c,c}^{(AJB)} \right)^{-1} = \mathbf{Z}_{c,c}^{(AJB)} = \begin{bmatrix} \mathbf{Z}_{c,c}^{(A)} + \mathbf{Z}_{c^{(A)},c^{(A)}}^{(J)} & -\mathbf{Z}_{c^{(A)},c^{(B)}}^{(J)} \\ -\mathbf{Z}_{c^{(B)},c^{(A)}}^{(J)} & \mathbf{Z}_{c,c}^{(B)} + \mathbf{Z}_{c^{(B)},c^{(B)}}^{(J)} \end{bmatrix} \tag{A.1}$$

This method was proposed in earlier publications such as [47–49] and later formulated in a much more compact and intuitive manner, the so-called in-situ identification [50–52]. *Inverse Substructuring* assumes that all joint information can be obtained by looking only at the connecting DoFs of the substructures, which are the elements on the off-diagonal matrices in $\mathbf{Z}_{c,c}^{(AJB)}$. When using *Inverse Substructuring* to identify the joint, one assumes that the complete model is extracted when $\mathbf{Z}_{c^{(A)},c^{(B)}}^{(J)}$ is found. Such an assumption then states that $\mathbf{Z}_{c^{(A)},c^{(A)}}^{(J)} = \mathbf{Z}_{c^{(B)},c^{(A)}}^{(J)} = \mathbf{Z}_{c^{(B)},c^{(B)}}^{(J)} = \mathbf{Z}_{c^{(A)},c^{(B)}}^{(J)}$, which is true when only simple node-to-node connection exist from one side to the other of the interface and the joint mass is negligible. The advantages and limitations of this method were shown and discussed in [30,31].

The estimated stiffness values for the *Inverse Substructuring* approach were obtained from Eq. (A.1). Here, the two off-diagonal matrices $\mathbf{Z}_{c^{(A)},c^{(B)}}^{(J)}$ and $\mathbf{Z}_{c^{(B)},c^{(A)}}^{(J)}$ are investigated. Their elements link the two substructures and should be identical in ideal cases. They are square matrices of the size of the number of VP DoFs. As described in Section 2, each coefficient in $\mathbf{Z}^{(J)}$ belongs to a coupling between a pair of DoFs with a stiffness value. Here, only the elements relative to the coupling between the DoFs in z -direction on each side of the interface, $k_z^{(J)}$, are investigated. Fig. A.11 shows the $k_z^{(J)}$ as a function of frequency that were extracted from the two off-diagonal matrices. Comparison of the two $k_z^{(J)}$ shows some discrepancies, which are more distinctive the less IDMs are considered. This behavior indicates that 2 IDMs might not be enough to describe the interface over the investigated frequency range, thus leading to wrong stiffness estimations. 4 and 6 IDMs seem to be able to better describe the interface. Although they show lots of spikes, which can be due to an amplification of measurement noise, the graphs show a constant trend, which is commonly expected from translational stiffness values. The increase in noise can be explained with the increase in IDMs. The more IDMs are considered, especially rotational ones, the more likely the results are noise polluted.

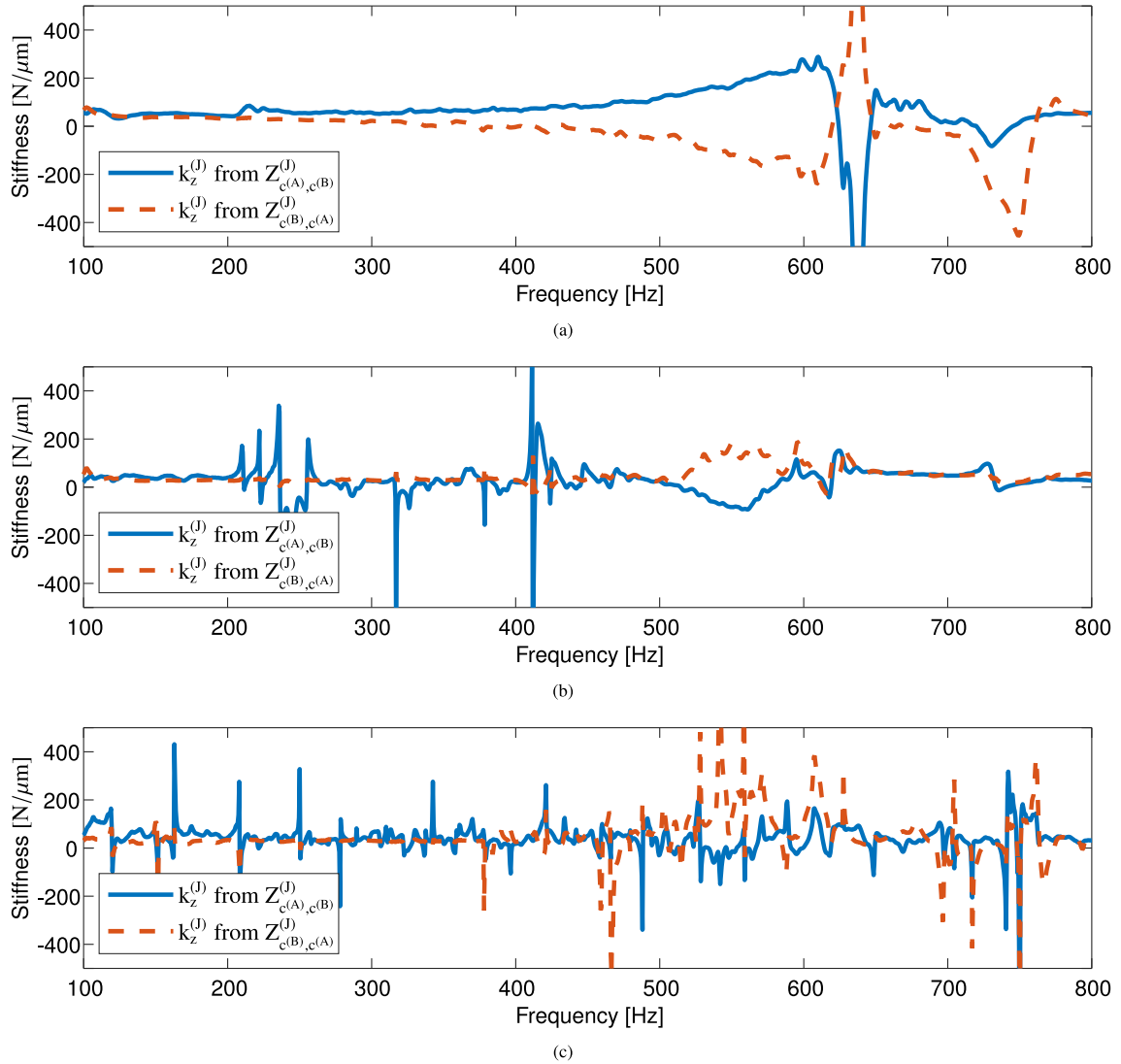


Fig. A.11. Stiffness estimation from Inverse Substructuring: (a) 2 IDMs (b) 4 IDMs (c) 6 IDMs.

A.2. Primal decoupling

Primal Decoupling [26], describes the idea visualized in Fig. 1b. It simply subtracts the parts from its assembly. With the assumption that measurements are performed only at the interface DoFs c , this approach can be written as in Eq. (A.2).

$$\begin{bmatrix} Z_{c,c}^{(A)} + Z_{c(A),c(A)}^{(J)} & -Z_{c(A),c(B)}^{(J)} \\ -Z_{c(B),c(A)}^{(J)} & Z_{c,c}^{(B)} + Z_{c(B),c(A)}^{(J)} \end{bmatrix} - \begin{bmatrix} Z_{c,c}^{(A)} & 0 \\ 0 & Z_{c,c}^{(B)} \end{bmatrix} = \begin{bmatrix} Z_{c(A),c(A)}^{(J)} & -Z_{c(A),c(B)}^{(J)} \\ -Z_{c(B),c(A)}^{(J)} & Z_{c(B),c(B)}^{(J)} \end{bmatrix} \tag{A.2}$$

To achieve this, the measured admittance matrices need to be inverted to obtain the corresponding receptance matrices before the decoupling is performed. Eq. (A.2) stores the contact stiffness information multiple times, i.e. in all four sub-matrices. However, Primal Decoupling investigates only the two diagonal matrices $Z_{c(A),c(A)}^{(J)}$, and $Z_{c(B),c(B)}^{(J)}$, from which the substructures influence is eliminated. In contrast to (3) and (A.3), Eq. (A.2) does not require any assumptions on the mass in the joint.

The estimated stiffness values for the Primal decoupling approach were obtained from Eq. (A.2). The off-diagonal matrices $Z_{c(A),c(B)}^{(J)}$ and $Z_{c(B),c(A)}^{(J)}$ are the same as for the Inverse Substructuring, thus the focus lies on the diagonal matrices $Z_{c(A),c(A)}^{(J)}$ and $Z_{c(B),c(B)}^{(J)}$. Fig. A.12 shows the results of the corresponding $k_z^{(J)}$ over the frequency range for the different IDMs. The $k_z^{(J)}$ extracted from $Z_{c(A),c(A)}^{(J)}$ is in general less smooth than the $k_z^{(J)}$ extracted from $Z_{c(B),c(B)}^{(J)}$. An explanation is that, for the Primal Decoupling, also the substructures need to be fully described by the IDMs within the frequency range of interest to eliminate their influence on the assembly. The

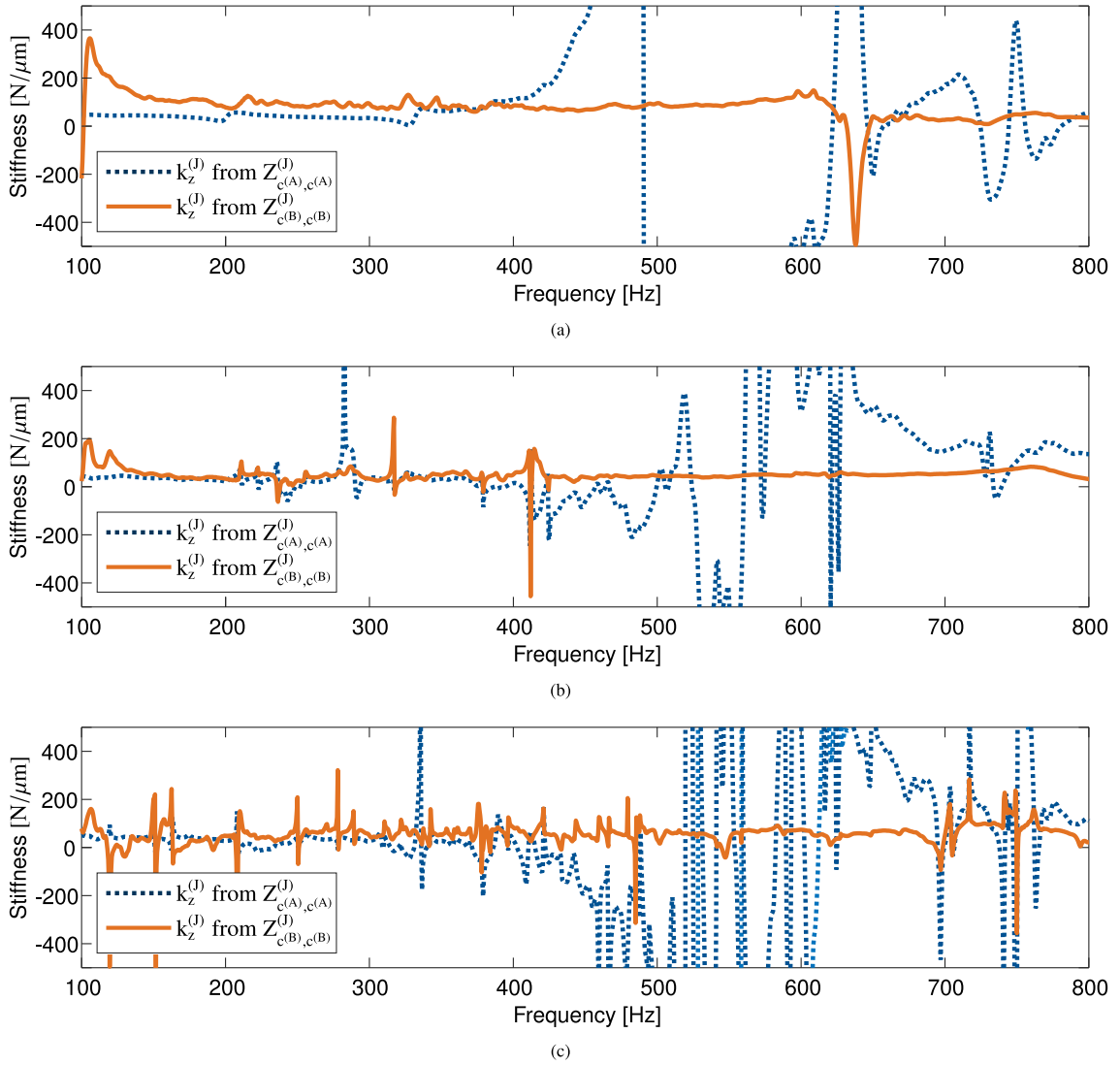


Fig. A.12. Stiffness estimation from Primal Decoupling (a) 2 IDMs, (b) 4 IDMs, (c) 6 IDMs.

results indicate that the IDMs cannot describe substructure A sufficiently at higher frequencies, thus, leading to wrong results. This is most likely due to the appearance of flexible modes of substructure A at higher frequencies, which are not considered in this study. In comparison, substructure B is the stiffer one and can be better described by the reduced data than substructure A and, thus can be better eliminated. The graphs of the $k_z^{(J)}$ extracted from $Z_{c^{(B)},c^{(B)}}^{(J)}$ show a constant trend. The noise issue for more IDMs mentioned in Appendix A.1 is visible here as well.

A.3. Decoupling interface DoFs

This section investigates the results of Eq. (A.3) where only interface DoFs are used for a decoupling.

$$Y^{(J)} = -BYB^T - BYB^T(-B\Delta YB^T)^{-1}BYB^T \quad \text{with} \quad \Delta Y = Y^{(AJB)} - Y \quad (\text{A.3})$$

Eq. (A.3) was proposed by [36] and its terms can be rewritten as in Eq. (A.4). This is done to make the properties of Eq. (A.3) more visible. The interface DoFs are denoted with the subscript c . The subscript $c^{(S)}$ describes interface DoFs in the assembly on structure S.

$$BYB^T = Y_{c,c}^{(A)} + Y_{c,c}^{(B)} \quad \text{and} \quad (-B\Delta YB^T)^{-1} = \left(Y_{c,c}^{(A)} + Y_{c,c}^{(B)} - Y_{c^{(A)},c^{(A)}}^{(AJB)} + Y_{c^{(A)},c^{(B)}}^{(AJB)} + Y_{c^{(B)},c^{(A)}}^{(AJB)} - Y_{c^{(B)},c^{(B)}}^{(AJB)} \right)^{-1} \quad (\text{A.4})$$

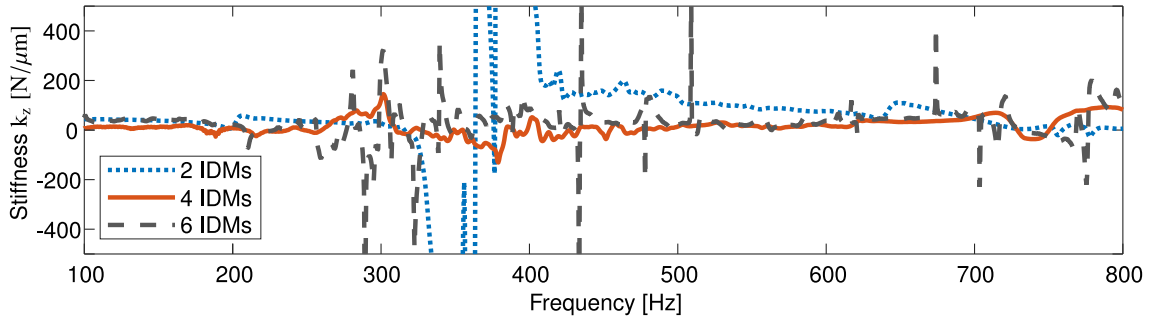


Fig. A.13. Decoupling when using only interface DoFs.

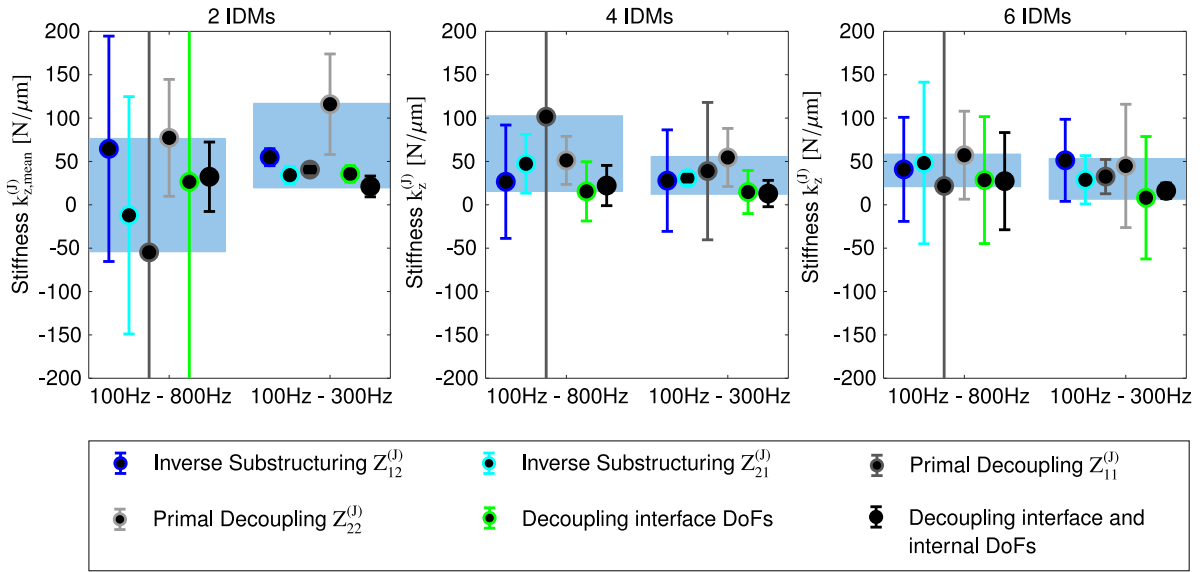


Fig. A.14. Comparison of the $k_z^{(J)}$ distribution for two different frequency ranges with standard deviation as error bars. The colored background bounds minimum and maximum value of each investigated case.

Eq. (A.4) shows that, due to the summation through the Boolean matrix \mathbf{B} , only the interface DoFs remain and contribute to $\mathbf{Y}^{(J)}$. Furthermore, it can be seen that the joint information is compressed. While $\mathbf{Y}^{(AJB)}$ stores the interface DoFs, and thus the joint properties multiple times, $\mathbf{Y}^{(J)}$ from Eq. (A.3) contains them only once, since all the remaining elements from $\mathbf{Y}^{(AJB)}$ that contain joint information are summed up. In order to obtain the frequency dependent contact stiffness matrix $\mathbf{K}^{(J)}$ from $\mathbf{Y}^{(J)}$, the latter matrix needs to be inverted and its real part determined. Eq. (A.3) is referred to as *decoupling interface DoFs* to highlight that the joint properties are obtained only from interface admittances in the assembled and decoupled state.

The previous two approaches give two $k_z^{(J)}$ from two submatrices. With this decoupling approach, only one $k_z^{(J)}$ per IDM case can be identified. The stiffness values are plotted in Fig. A.13 for the three cases of IDM numbers, showing that, for frequencies up to 250 Hz, all cases have a clear constant trend. Afterwards, they become less smooth. Here, the 2 IDM case shows very high variations whereas the other two cases somehow keep oscillating around a mean value.

A.4. Comparison of the substructuring approaches

As done in Section 5, two different frequency ranges are used for determining $k_{z,mean}^{(J)}$. However, the former used frequency range 300 Hz – 600 Hz is replaced by the range of 100 Hz – 300 Hz because it is more suitable to exclude noise. The 100 Hz – 800 Hz range stays untouched. The mean $k_{z,mean}^{(J)}$ over these two spectrums are shown in Fig. A.14 together with their standard deviations, plotted as error bars. The colored background bounds minimum and maximum value of each investigated case. For comparison, the results of *decoupling interface and internal DoFs* are presented too. Fig. A.14 shows that the overall extracted stiffness values are in a range of $-55 \text{ N}/\mu\text{m}$ and $116 \text{ N}/\mu\text{m}$. Note that negative stiffness values are unphysical here as they indicate an active system. Their appearance is due to an insufficient description of the interface since they only appear for the 2 IDM case. Furthermore, the stiffness values are more spread when only 2 IDMs are considered, regardless of the used approach, suggesting that only 2 IDMs

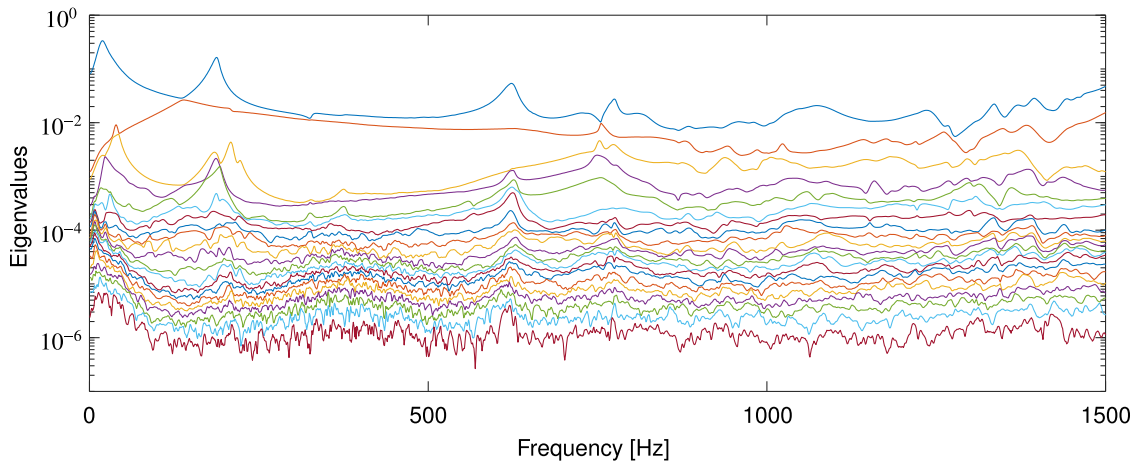


Fig. B.15. Singular Value Decomposition (SVD) of $Y^{(AJB)} - Y$, which is the matrix that describes the joint. Each line (color) represents one singular value. The corresponding modes can be estimated by looking at the eigenvectors in U .

are not adequate to describe the investigated system. Fig. A.14 also shows that the frequency range chosen for contact parameter estimation has an influence on the extracted stiffness values. For a poorly described interface (i.e. 2 IDMs), this influence can be significant while for better described interfaces the influence is less distinctive. It is concluded that the choice of the IDMs needed to describe the interface has the greatest influence on the extracted $k_{z,mean}^{(J)}$. Better descriptions of the interface's movement (IDMs) and of the (sub)structures lead to more reliable results.

In terms of approaches, it was found that *Inverse Structuring* is relatively easy and fast to implement since it does not need the FRFs of the individual substructures, thus halving the required measurement data compared to the other investigated decoupling approaches. However, this approach is only recommended when the interface behavior and thus, the needed IDMs are known (e.g. for the 4 IDM and 6 IDM case in this study). The cleanest and most reliable results are instead obtained when a decoupling with both interface and internal DoFs is conducted, but it is the most time-consuming approach in terms of required measurement data.

Appendix B. Determination of interface displacement modes (IDMs) with Singular Value Decomposition (SVD)

When using a VPT, it is beneficial to know how many modes are needed to describe the system sufficiently and which modes they are. One possibility to investigate these questions is by looking at the eigenvalues and eigenvectors of the joint via a Singular Value Decomposition (SVD).

$$A(\omega) = U(\omega)S(\omega)V^T(\omega) \quad (\text{B.1})$$

The SVD splits any matrix into three matrices: U , S , V , where S is a diagonal matrix storing the singular values and U and V are orthogonal matrices. With A storing FRFs, a SVD of A at a specific frequency gives information on the response modes stored as columns in U and excitation modes stored as columns in V . This investigation does not require measurements of the joint directly because use of the following can be taken: The difference between the measured FRFs of the assembly $Y^{(AJB)}$ and the measured FRFs of the substructures (stored in block-diagonal form in Y) gives information of the joint. Thus, a SVD of $Y^{(AJB)} - Y$ can indicate the number of eigenvalues dominant in the joint, i.e. how many modes are needed to describe the joint. Fig. B.15 shows the singular values of the joint, i.e. the elements in S for a SVD decomposition of $Y^{(AJB)} - Y$. Two modes are dominant up to approx. 750 Hz before more modes gain importance. This is a typical behavior as at higher frequencies also flexible modes appear. The corresponding modes can be estimated by looking at the columns in U and using the information of the corresponding sensor locations. The first column in U belongs to the dominant eigenvalue, the second column to the second eigenvalue and so on. It is to mention that a line does not necessarily represent one and the same mode over the whole frequency range, meaning that the modes that are dominant at lower frequencies do not need to be the same as the one at higher. A range of 0–800 Hz was investigated. It could be seen that the modes corresponding to the dominant eigenvalue show either a vertical movement or a lateral movement. The modes belonging to the second dominant eigenvalue show a lateral or horizontal movement (for convention of the directions see Fig. 2a).

Appendix C. Investigation of low frequency noise in dynamic stiffness

The dynamic stiffness matrix Z , from which the stiffness k can be extracted, is obtained from an admittance matrix Y by inversion (see Eq. (2)). For simplification, a 1D problem is here considered. Assuming the FRF could be measured without any measurement noise, the corresponding Z would look like the red curve in Fig. C.16b. At low frequencies, the stiffness is dominant, recognizable

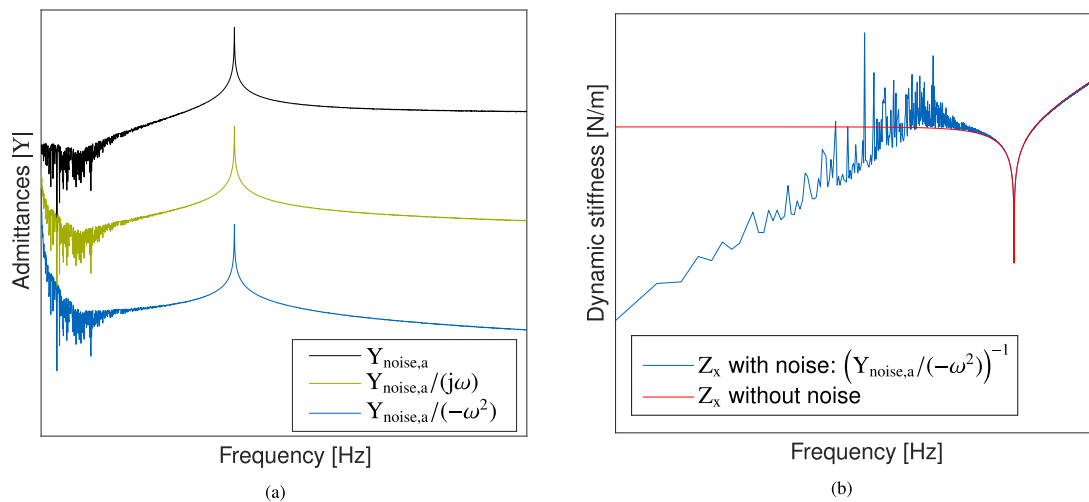


Fig. C.16. Investigation of low frequency noise in dynamic stiffness: (a) Integration of acceleration FRF with noise floor (b) Dynamic stiffness of a two times integrated acceleration FRF without noise and with noise contribution.

on the constant “stiffness line”, before the mass gains importance and leads to the drop before the curve increases. In reality, measurement noise is present and included in the measured FRF. When the FRF is measured with an accelerometer, it needs to be integrated twice, which means divided by ω^2 , to obtain the dynamic stiffness Z . This division dramatically amplifies the noise in the lower frequency range (Fig. C.16a), creating an increase of the “displacement FRF” as omega goes to zero, whereas the FRF for displacement should be constant close to omega zero. That erroneous FRF behavior at low frequency will then generate a Z that is decreasing as omega approaches zero (blue curve in Fig. C.16b). A stiffness estimation from this slope is not possible. For velocity FRFs this behavior should be less pronounced since the Y is only divided by ω and not ω^2 to obtain the Z . If the measurement noise is too dominant, it can happen that no “stiffness line” can be extracted before the mass influence occurs.

References

- [1] W. Sextro, *Dynamical Contact Problems with Friction*, Springer Berlin Heidelberg, Berlin, Heidelberg, 2007, <http://dx.doi.org/10.1007/978-3-540-45317-8>.
- [2] D.J. Ewins, A survey of contact hysteresis measurement techniques, in: *Mech. Jointed Struct.*, Springer International Publishing, Cham, 2018, pp. 149–179, http://dx.doi.org/10.1007/978-3-319-56818-8_12.
- [3] M. Lavella, D. Botto, M.M. Gola, Design of a high-precision, flat-on-flat fretting test apparatus with high temperature capability, *Wear* 302 (2013) 1073–1081, <http://dx.doi.org/10.1016/j.wear.2013.01.066>.
- [4] A. Fantetti, C. Pennisi, D. Botto, S. Zucca, C. Schwingshackl, Comparison of contact parameters measured with two different friction rigs for nonlinear dynamic analysis, in: *Proc. ISMA 2020 - Int. Conf. Noise Vib. Eng. USD*, 2020, 2165–2174.
- [5] T. Hoffmann, L. Panning/von Scheidt, J. Wallaschek, Analysis of contacts in friction damped turbine blades using dimensionless numbers, *Eng. Gas Turbines Power* 141 (12) (2019) <http://dx.doi.org/10.1115/1.4044481>.
- [6] A.R. Warmuth, P.H. Shipway, W. Sun, Fretting wear mapping: The influence of contact geometry and frequency on debris formation and ejection for a steel-on-steel pair, *Proc. R. Soc. A* (2015) <http://dx.doi.org/10.1098/rspa.2014.0291>.
- [7] M.E. Kartal, D.M. Mulvihill, D. Nowell, D.A. Hills, Determination of the frictional properties of titanium and nickel alloys using the digital image correlation method, *Exp. Mech.* 51 (3) (2011) 359–371, <http://dx.doi.org/10.1007/s11340-010-9366-y>.
- [8] J. Hintikka, A. Lehtovaara, A. Mantyla, Fretting-induced friction and wear in large flat-on-flat contact with quenched and tempered steel, *Tribol. Int.* 92 (2015) 191–202, <http://dx.doi.org/10.1016/j.triboint.2015.06.008>.
- [9] A. Fantetti, C. Schwingshackl, Effect of friction on the structural dynamics of built-up structures: An experimental study, in: *Vol. 11 Struct. Dyn. Struct. Mech. Vib. Damping: Supercrit. CO2*, American Society of Mechanical Engineers, 2020, <http://dx.doi.org/10.1115/GT2020-14945>.
- [10] J. de Crevoisier, N. Swiergiel, L. Champaney, F. Hild, Identification of in situ frictional properties of bolted assemblies with digital image correlation, *Exp. Mech.* 52 (6) (2012) 561–572, <http://dx.doi.org/10.1007/s11340-011-9518-8>.
- [11] M. Kartal, D. Mulvihill, D. Nowell, D. Hills, Measurements of pressure and area dependent tangential contact stiffness between rough surfaces using digital image correlation, *Tribol. Int.* 44 (10) (2011) 1188–1198, <http://dx.doi.org/10.1016/j.triboint.2011.05.025>.
- [12] D.M. Mulvihill, H. Brunskill, M.E. Kartal, R.S. Dwyer-Joyce, D. Nowell, A comparison of contact stiffness measurements obtained by the digital image correlation and ultrasound techniques, *Exp. Mech.* 53 (7) (2013) 1245–1263, <http://dx.doi.org/10.1007/s11340-013-9718-5>.
- [13] J. De Pauw, W. De Waele, R. Hojjati-Talemi, P. De Baets, On the use of digital image correlation for slip measurement during coupon scale fretting fatigue experiments, *Int. J. Solids Struct.* 51 (18) (2014) 3058–3066, <http://dx.doi.org/10.1016/j.ijsolstr.2014.05.002>.
- [14] W. Chen, M. Jin, I. Lawal, M.R. Brake, H. Song, Measurement of slip and separation in jointed structures with non-flat interfaces, *Mech. Syst. Signal Process.* 134 (2019) 106325, <http://dx.doi.org/10.1016/j.ymsp.2019.106325>.
- [15] R.S. Dwyer-Joyce, B.W. Drinkwater, A.M. Quinn, The use of ultrasound in the investigation of rough surface interfaces, *J. Tribol.* 123 (1) (2001) 8–16, <http://dx.doi.org/10.1115/1.1330740>.
- [16] J.Y. Kim, A. Baltazar, S.I. Rokhlin, Ultrasonic assessment of rough surface contact between solids from elastoplastic loading-unloading hysteresis cycle, *J. Mech. Phys. Solids* 52 (8) (2004) 1911–1934, <http://dx.doi.org/10.1016/j.jmps.2004.01.006>.

- [17] J.M. Baik, R.B. Thompson, Ultrasonic scattering from imperfect interfaces: A quasi-static model, *J. Nondestruct. Eval.* 4 (3–4) (1984) 177–196, <http://dx.doi.org/10.1007/BF00566223>.
- [18] G. Starzynski, R. Buczkowski, Ultrasonic measurements of contact stiffness between rough surfaces, *J. Tribol.* 136 (3) (2014) <http://dx.doi.org/10.1115/1.4027132>.
- [19] A. Fantetti, S. Mariani, L. Pesaresi, D. Nowell, F. Cegla, C. Schwingshackl, Ultrasonic monitoring of friction contacts during shear vibration cycles, *Mech. Syst. Signal Process.* 161 (2021) <http://dx.doi.org/10.1016/j.ymssp.2021.107966>.
- [20] R. Sahli, G. Pallares, C. Ducottet, I.E. Ben Ali, S. Al Akhrass, M. Guibert, J. Scheibert, Evolution of real contact area under shear and the value of static friction of soft materials, *Proc. Natl. Acad. Sci. USA* 115 (3) (2018) 471–476, <http://dx.doi.org/10.1073/pnas.1706434115>.
- [21] B.A. Krick, J.R. Vail, B.N. Persson, W.G. Sawyer, Optical in situ micro tribometer for analysis of real contact area for contact mechanics, adhesion, and sliding experiments, *Tribol. Lett.* 45 (1) (2012) 185–194, <http://dx.doi.org/10.1007/s11249-011-9870-y>.
- [22] O. Ben-David, S.M. Rubinstein, J. Fineberg, Slip-stick and the evolution of frictional strength, *Nature* 463 (7277) (2010) 76–79, <http://dx.doi.org/10.1038/nature08676>.
- [23] H. Ahmadian, H. Jalali, Identification of bolted lap joints parameters in assembled structures, *Mech. Syst. Signal Process.* 21 (2) (2007) 1041–1050, <http://dx.doi.org/10.1016/j.ymssp.2005.08.015>.
- [24] G. Zhao, Z. Xiong, X. Jin, L. Hou, W. Gao, Prediction of contact stiffness in bolted interface with natural frequency experiment and FE analysis, *Tribol. Int.* 127 (2018) 157–164, <http://dx.doi.org/10.1016/j.triboint.2018.05.044>.
- [25] D.D. Klerk, D.J. Rixen, S.N. Voormeeren, General framework for dynamic substructuring: History, review and classification of techniques, *AIAA J.* 46 (5) (2008) 1169–1181, <http://dx.doi.org/10.2514/1.33274>, URL <http://arc.aiaa.org/doi/10.2514/1.33274>.
- [26] M. Van der Seijs, *Experimental Dynamic Substructuring Analysis and Design Strategies for Vehicle Development Maarten van der Seijs (Ph.D. thesis)*, 2016.
- [27] J.R. Crowley, A.L. Klosterman, G.T. Rocklin, H. Vold, Direct structural modification using frequency response functions, in: *Proceedings of II International Modal Analysis Conference (IMAC)*, Orlando, FL. Society of Experimental Mechanics. Bethel, CT, Feb. 1984.
- [28] B. Jetmundsen, R.L. Bielawa, W.G. Flannely, Generalized frequency domain substructure synthesis, *J. Am. Helicopter Soc.* 33 (1) (1988) 55–64, <http://dx.doi.org/10.4050/jahs.33.1.55>.
- [29] J. Brunetti, W. D'Ambrogio, A. Fregolent, Dynamic coupling of substructures with sliding friction interfaces, *Mech. Syst. Signal Process.* 141 (2020) 106731, <http://dx.doi.org/10.1016/j.ymssp.2020.106731>.
- [30] M. Haeussler, S.W. Klaassen, D.J. Rixen, Experimental twelve degree of freedom rubber isolator models for use in substructuring assemblies, *J. Sound Vib.* 474 (June) (2020) <http://dx.doi.org/10.1016/j.jsv.2020.115253>.
- [31] J. Meggitt, *On In-Situ Methodologies for the Characterisation and Simulation of Vibro-Acoustic Assemblies (Ph.D. thesis)*, University of Salford (United Kingdom), 2017.
- [32] A.E. Mahmoudi, C.H. Meyer, D.J. Rixen, Comparison of different approaches to include connection elements into frequency based substructuring, *Exp. Tech.* 44 (4) (2020) 425–433, <http://dx.doi.org/10.1007/s40799-020-00360-1>.
- [33] Ş. Tol, H.N. Özgüven, Dynamic characterization of structural joints using FRF decoupling, in: *Topics in Modal Analysis I*, Vol. 5, Springer, New York, 2012, pp. 435–446, http://dx.doi.org/10.1007/978-1-4614-2425-3_41.
- [34] Ş. Tol, H.N. Özgüven, Dynamic characterization of bolted joints using FRF decoupling and optimization, *Mech. Syst. Signal Process.* 54 (2015) 124–138, <http://dx.doi.org/10.1016/j.ymssp.2014.08.005>.
- [35] S.W. Klaassen, M.V. van der Seijs, D. de Klerk, System equivalent model mixing, *Mech. Syst. Signal Process.* 105 (2018) 90–112, <http://dx.doi.org/10.1016/j.ymssp.2017.12.003>.
- [36] S.W.B. Klaassen, D.J. Rixen, Using SEMM to identify the joint dynamics in multiple degrees of freedom without measuring interfaces, in: *Conf. Proc. Soc. Exp. Mech. Ser.*, 2020, pp. 87–99, http://dx.doi.org/10.1007/978-3-030-12184-6_10.
- [37] M.S. Allen, D.J. Rixen, M. van der Seijs, P. Tiso, T.J.S. Abrahamsson, R.L. Mayes, *Substructuring in Engineering Dynamics*, Vol. 594, Springer, 2020, <http://dx.doi.org/10.1007/978-3-030-25532-9>.
- [38] S.N. Voormeeren, D.J. Rixen, A family of substructure decoupling techniques based on a dual assembly approach, *Mech. Syst. Signal Process.* 27 (1) (2012) 379–396, <http://dx.doi.org/10.1016/j.ymssp.2011.07.028>.
- [39] A. Fantetti, L.R. Tamatam, M. Volvert, I. Lawal, L. Liu, L. Salles, M.R. Brake, C.W. Schwingshackl, D. Nowell, The impact of fretting wear on structural dynamics: Experiment and simulation, *Tribol. Int.* 138 (2019) 111–124, <http://dx.doi.org/10.1016/j.triboint.2019.05.023>.
- [40] J. Maierhofer, A.E. Mahmoudi, D.J. Rixen, Development of a low cost automatic modal hammer for applications in substructuring, in: *Dynamic Substructures*, Vol. 4, Springer International Publishing, Cham, 2020, pp. 77–86, http://dx.doi.org/10.1007/978-3-030-12184-6_9.
- [41] P. Avitabile, *Modal Testing a Practitioner's Guide*, John Wiley & Sons Ltd, 2018, <http://dx.doi.org/10.1002/9781119222989>.
- [42] J. Wang, T. Chen, X.P. Wang, Y. Xi, Dynamic identification of tangential contact stiffness by using friction damping in moving contact, *Tribol. Int.* 131 (2019) 308–317, <http://dx.doi.org/10.1016/j.triboint.2018.10.028>.
- [43] K.H. Koh, J.H. Griffin, S. Filippi, A. Akay, Characterization of turbine blade friction dampers, *J. Eng. Gas Turbines Power* 127 (4) (2005) 856–862, <http://dx.doi.org/10.1115/1.1926312>.
- [44] J. Wu, R. Yuan, Z. He, D. Zhang, Y. Xie, Experimental study on dry friction damping characteristics of the steam turbine blade material with nonconforming contacts, *Adv. Mater. Sci. Eng.* 2015 (2015) <http://dx.doi.org/10.1155/2015/849253>.
- [45] R.L. Mayes, M. Arviso, *Design studies for the transmission simulator method to generate experimental dynamic substructures*, in: *International Semin. Modal Anal.*, 2010, pp. 1929–1938.
- [46] E.A. Pasma, M.V.V.D. Seijs, S.W.B. Klaassen, M.W.V.D. Kooij, Frequency based substructuring with the virtual point transformation, flexible interface modes and a transmission simulator, in: Linderholt A., Allen M., Mayes R., Rixen D. (eds) *Dynamics of Coupled Structures*, Volume 4. Conference Proceedings of the Society for Experimental Mechanics Series. Springer, Cham., 2018, pp. 205–213, http://dx.doi.org/10.1007/978-3-319-74654-8_18.
- [47] J. Zhen, T.C. Lim, G. Lu, Determination of system vibratory response characteristics applying a spectral-based inverse sub-structuring approach. Part I: analytical formulation, *Int. J. Veh. Noise Vib.* 1 (1–2) (2004) 1–30, <http://dx.doi.org/10.1504/ijvnv.2004.004066>.
- [48] J. Zhen, T.C. Lim, G. Lu, Determination of system vibratory response characteristics applying a spectral-based inverse substructuring approach. Part II: motor vehicle structures, *Int. J. Veh. Noise Vib.* 1 (1–2) (2004) 31–67, <http://dx.doi.org/10.1504/ijvnv.2004.004066>.
- [49] Z.W. Wang, J. Wang, Inverse substructure method of three-substructures coupled system and its application in producttransport-system, *J. Vib. Control* 17 (6) (2011) 943–951.
- [50] A. Moorhouse, A.S. Elliot, Y. Heo, Intrinsic characterisation of structure-borne sound sources and isolators from in-situ measurements, in: *Proc. Meet. Acoust.*, Vol. 19, 2013, <http://dx.doi.org/10.1121/1.4799691>.
- [51] J.W. Meggitt, A.S. Elliott, A.T. Moorhouse, H.K. Lai, In situ determination of dynamic stiffness for resilient elements, *Proc. Inst. Mech. Eng. C J. Mech. Eng. Sci.* 230 (6) (2016) 986–993, <http://dx.doi.org/10.1177/0954406215618986>.
- [52] L. Keersmaekers, L. Mertens, R. Penne, P. Guillaume, G. Steenackers, Decoupling of mechanical systems based on insitu frequency response functions: The link-preserving, decoupling method, *Mechanical Systems and Signal Processing* 58 (2015) 340–354, <http://dx.doi.org/10.1016/j.ymssp.2014.11.016>.